Energy transfer in nanotube-chromophore complexes

Im Fachbereich Physik der
Freien Universität Berlin
eingereichte

Dissertation

von

Friederike Ernst

Berlin, im Juni 2013

1. Gutachter: Prof. Dr. Stephanie Reich
2. Gutachter: Prof. Dr. José Ignacio Pascual

Tag der Einreichung: 13. Juni 2013
Tag der Disputation: 20. September 2013

Eidesstattliche Erklärung

Hiermit versichere ich, daß ich alle verwendeten Hilfsmittel und Hilfen angegeben und die vorliegende Arbeit auf dieser Grundlage selbstständig verfasst habe. Diese Arbeit ist nicht schon einmal in einem früheren Promotionsverfahren eingereicht worden.

Friederike Ernst

Kurzfassung

Die vorliegende Arbeit befasst sich mit der Herstellung von Energietransfersystemen aus Nanoröhren und Farbstoffen, und deren Charakterisierung mithilfe optischer Methoden. Die Nanoröhren-Farbstoffkomplexe werden gebildet indem eine chromophore Einheit, hier ein Perylenderivat, in das Tensid, das die Nanoröhre in Lösung hält, eingebaut wird. Das Perylen setzt sich über eine Interaktion der π-Orbitale der Nanoröhre mit den π-Orbitalen des Farbstoffes nicht-kovalent auf die Wand der Nanoröhre. Diese räumliche Nähe ermöglicht einen Förster-Resonanzenergietransferprozess mit einem Abstand zwischen Donor und Akzeptor weit unterhalb des Förster-Radius, und dementsprechend mit einer Transfereffizienz nahe eins. Der Energietransfer beruht auf einer Dipol-Dipol Wechselwirkung, die die intrinischen optoelektronischen Eigenschaften der Nanoröhre nicht ändert, aber einen neuen Anregungskanal über die Absorptionsbande der Chromophore eröffnet. Dieser zusätzliche Anregungskanal wird durch Photolumineszenzmessungen charakterisiert.

Zehn funktionale Tenside wurden entworfen, alle mit ähnlichem chromophoren Kern, jedoch mit verschiedenartigen hydrophoben Einheiten für Wasserlöslichkeit sowie unterschiedlichen Alkylketten für die Individualisierung der Röhren. Die zehn Moleküle unterscheiden sich in ihrer Eignung als Tensid und in ihrer Neigung, Energietransferkomplexe mit den Nanoröhren zu formen. Mit diesen Daten können wir einen Leitfaden für das Design funktionaler Tenside aufstellen. Die Transfereffizienzen und Anregungscharakteristiken der Energietransferkomplexe werden analysiert und geben Aufschluss über die Morphologie der Chromophorenadsorption auf der Nanoröhre.

Alle Nanoröhrenproben, die mit Perylenderivattensiden solubilisiert werden, weisen eine von herkömmlichen Tensiden abweichende Lumineszenzintensitätsverteilung über die Chiralitäten auf. Der physikalische Mechanismus hinter dieser chiralitätsspezifischen Luminenszenzverstärkung wird durch resonante Ramanprofile sowie das Schwellen von mit Gallensäurentensid solubilisierten Nanoröhren mit organischen Lösungsmitteln und verschiedenen Farbstoffen ergründet. Diese Daten lassen darauf schließen, daß sowohl

präferenzielle Solubiliserung durch das Perylenderivattensid als auch chiralitätsspezifische verbesserte Entbündelung durch die enthaltene aromatische Moietät zu den Unterschieden gegenüber der Lumineszenzintensitätsverteilung mit Gallensäurentensid solubilisierter Nanoröhren beitragen.

Abstract

In this thesis we create nanotube-chromophore energy transfer systems and characterize them optically. The nanotube-chromophore complexes are devised through the incorporation of a chromophoric perylene derived unit into the surfactant. The functional perylene unit π-π stacks on the nanotube wall. This close proximity results in a Förster resonance energy transfer at a distance much smaller than the Förster radius from the dye into the tube, yielding transfer efficiencies of almost unity. The energy transfer is mediated by a dipole-dipole interaction which does not alter the nanotube's intrinsic optoelectronic properties, but opens an additional channel for the excitation of the nanotube in the absorption band of the chromophore. This additional channel is characterized through photoluminescence measurements.

Ten functional surfactants were designed, all featuring a similar chromophoric core. The hydrophobic units for water solubility and alkyl chains for nanotube individualization were varied. All surfactants differ in their individualization capabilities as well as their propensity for forming energy transfer complexes. This approach yields a guideline for the tailored design of functional surfactants. The efficiencies and excitation characteristics of the energy transfer complexes are analyzed to shed light on the morphology of the chromophore adsorption on the nanotube.

All samples solubilized with a perylene-based surfactant show an altered luminescence intensity pattern across the chiralities. The mechanism behind this chirality specific luminescence intensity enhancement is investigated through resonant Raman profiles, as well as swelling of bile salt suspended nanotubes with organic solvents and chromophores. These measurements indicate that both preferential solubilization and chirality-specific enhanced debundling through the aromatic moiety are responsible for the differences between perylene-based surfactants and bile salts.

Contents

1 | Motivation

Carbon nanotubes have held the fascination of the scientific community in the two decades since their discovery in 1991 for two reasons: For one, they are the epitome of a truly one dimensional material and, consequently, an ideal test bed for the behavior of low-dimensional systems. Dimensionality plays a large role in many fundamental concepts in solid state physics. For instance, in 1D systems the density of states does not follow a $\sqrt{E}$ behavior as in a single band in bulk, or a stepped function like in 2D materials. The density of states in 1D systems is characterized by a sequence of peaks followed by a $1/\sqrt{E}$ behavior, see Sec. 2.1.1. Consequently, unlike in higher dimensional systems, optical transitions between higher excited electronic states are generally well defined. Lack of charge screening in 1D systems leads to extraordinarily high excitonic binding energies on the order of several 100 meV, causing the actual single particle band structure to retreat into the background, and being replaced by the corresponding excitonic bands, see Sec. 2.1.2. While these and other features characteristic of 1D physics have been explained, the jury is still out on several more. For instance, the question whether charge carriers in metallic 1D materials obey Fermi-Dirac statistics or whether they are better described by a Luttinger liquid remains open.[1] Equally unanswered as of yet is the question of whether phase transitions, such as in superconductivity, can take place in 1D systems at all.[2] So, without doubt, carbon nanotubes still harbor new physics.

The other reason nanotubes are extensively studied is for their potential applications. Carbon nanotubes are outstanding electrical and thermal conductors,[3; 4] they possess unsurpassed mechanical strength,[5] and they emit in the near infrared, a region important in biomedical applications owing to a spectral window of relative tissue transparency.[6]

This thesis comes out on both sides. While we closely characterize the complex quantum system formed by putting together nanotubes and chromophores optically in terms of fundamental physics, we are acutely aware of the potential applications of such systems. Nanotubes exhibit ballistic transport properties, but only interact with light of very specific energies, namely, where the energy for an allowed optical transition of the nanotube is

met. These energies are very different for different nanotube chiralities, see Sec. 2.1.1. Furthermore, the oscillator strength of carbon nanotubes at 0.01 per C-atom is much lower than that of many dyes.[7] Perylene for instance has a tenfold higher oscillator strength.[8] By combining both systems, we intended to tap the strengths of the nanotube, i. e., the ballistic transport properties, and the light-interaction properties of the chromophore. The ultra efficient energy transfer functionally linking the two systems boasts transfer efficiencies close to unity and was attained by non-covalent functionalization through a π-π stacking mechanism.[9; 10]

In nanotube technology, a big problem is posed by the inherent polydispersity of nanotube samples. Currently, it is not possible to grow monochiral samples, and ex-post separation is very inefficient, Sec. 2.1.4. Being able to excite all nanotube chiralities at the same energy, i. e., in the absorption band of the chromophore, is a large advantage for immensely promising devices such as nanotube based optical transistors. Nanotube field effect transistors have high on/off ratios, fast response times owed to extremely high mobilities, and can be made very small, in effect only limited by the size of the contact. This makes them a long-time favorite of nanotechnologists.[11; 12; 13] Using light instead of voltage as the gating parameter for a transistor is particularly appealing for applications for which speed is paramount. With the additional chromophoric excitation band in the nanotube-chromophore complexes, photocurrent can be generated with a single wavelength excitation for any nanotube chirality. Consequently, the tube used in an optical transistor can be of any semiconducting chirality. Efficient methods for separating nanotubes by electronic type have been reported repeatedly, see Sec. 2.1.4.

For the same reason, biomedical applications will also benefit from dye-sensitized nanotubes. Nanotubes can be used to deliver drugs precisely, or dispense heat highly locally upon irradiation in the near infrared, destroying targeted tissues.[6] Tracking nanotubes in biological surroundings is currently done with traditional fluorophores or radioactive labeling.[14] Traditional fluorophores are sizable, and thus counteract some of the much desired physical characteristics of the nanotube, i. e., their size, which allows them to be readily distributed in tissues. "Seeing" all nanotubes after irradiation at one wavelength without the cost of significantly increased size and the use of radioactive materials is preferable for reasons of simplicity, stability, and biocompatibility. In our studies, we have taken care to strive for biocompatibility, using for instance polyglycerol dendrons for the hydrophilic part of the designer surfactants. Polyglycerol dendrons are known to not interact with proteins, and are also used in the coating of non-fouling surfaces.[15]

Furthermore, dye-sensitization is potentially of tremendous interest for the solar cell

industry. Nanotubes can be sensitized with different dyes, covering the entire UV and visible excitation spectrum. The high optical cross section of the dye together with the ultra efficient energy transfer into the tube, followed by the ballistic transport in the nanotube itself, make this an ideal system for light-to-current conversion applications, especially when one considers that the creation of the nanotube-chromophore energy transfer complexes is achieved in solution and is consequently completely scalable.[9]

2 | Introduction

2.1. Carbon nanotubes

Carbon nanotubes were first discovered in 1991 by Sumio Ijima in their multiwalled form,[16] single walled carbon nanotubes were first reported two years later.[17; 18] Single walled nanotubes are hollow cylinders of sp^2 bonded carbon, their diameter is on the order of 1 nm with macroscopic lengths. While initially nanotubes were characterized with electron microscopy, it was quickly realized that the truly remarkable thing about them are their mechanical strength and optoelectronic properties. In 1992 Hamada *et al.* and Saito *et al.* showed through tight binding and zone folding calculations that the electronic structure of the nanotube crucially depends on the precise morphology of the tube due to quantum confinement effects perpendicular to the nanotube axis.[19; 20] Consequently, both metallic and semiconducting nanotubes exist.

Carbon nanotubes can be rationalized as rolled up graphene sheets, Fig 2.1. The tube formed by identifying the start and end points of the chiral vector $\mathbf{C}$ with each other is referred to as the (n, m) chirality, where $\mathbf{C} = n\mathbf{a}_1 + m\mathbf{a}_2$, and $\mathbf{a}_1$, $\mathbf{a}_2$ are the graphene lattice vectors. $\mathbf{C}$ is then simply the tube circumference. Two kinds of tubes exhibit a high degree of symmetry: Armchair tubes are of the (n, n) type with chiral angle $\theta = 30°$, zigzag tubes have $(n, 0)$ and, consequently, $\theta = 0°$, see Fig 2.1.

From the chirality both the diameter, d, and the chiral angle, θ, can be calculated easily:

$$\begin{aligned} d &= \frac{|\mathbf{C}|}{\pi} = \frac{a_0}{\pi}\sqrt{n^2 + nm + m^2} \\ \theta &= \arccos\frac{\mathbf{a}_1 \cdot \mathbf{C}}{|\mathbf{a}_1| \cdot |\mathbf{C}|} = \arccos\frac{n + m/2}{\sqrt{n^2 + nm + m^2}}, \end{aligned} \tag{2.1}$$

where a_0 is the length of the graphene lattice vector, 2.46 Å.

The unit cell length of a carbon nanotube varies tremendously depending on the

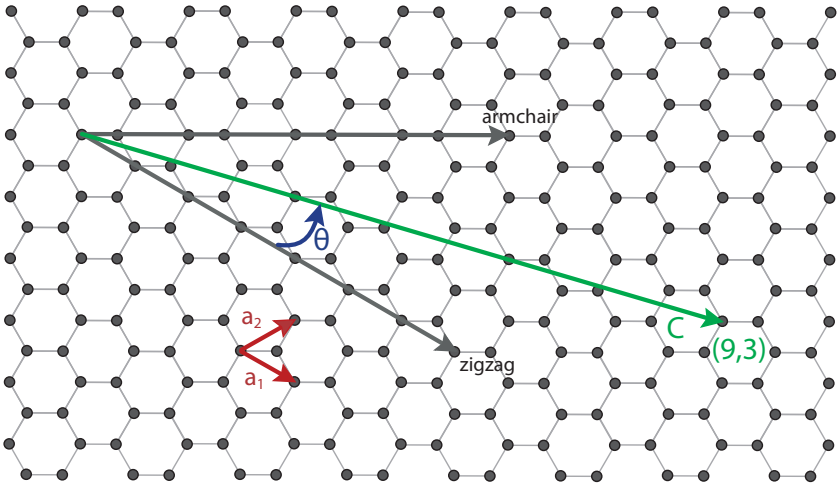

Figure 2.1. Carbon nanotube morphology: The circumference of any tube is the chiral vector $\mathbf{C}$. Here, $\mathbf{C} = 9\mathbf{a}_1 + 3\mathbf{a}_2$, and the resulting tube is thus known as (9,3). The angle between $\mathbf{a}_1$ and $\mathbf{C}$ is known as the chiral angle θ.

chirality, and is generally given by

$$a = \frac{\sqrt{n^2 + nm + m^2}}{n\mathcal{R}}, \tag{2.2}$$

where $\mathcal{R} = 3$ for (n-m)/3n integer and $\mathcal{R} = 1$ otherwise. For the full geometrical derivation see Ref. [21].

2.1.1. Nanotube band structure

The nanotube band structure is related to the graphene band structure. In the graphene dispersion relation, Fig. 2.2, conduction and valence bands touch in six points, known as the Dirac points, of which two are inequivalent, K and K'. The dispersion relation near the K points is linear, resulting in the conical structures called Dirac cones. The states close to the Fermi energy are in general also the states that contribute to the optoelectronic properties, hence it is the linear parts of the dispersion relation that govern the behavior of graphene for most of the relevant physical processes.

The nanotube band structure can be derived from the graphene band structure. The wave vectors along the tube axis, $k_{||}$, are identical to those of graphene. However, the wave vectors perpendicular to the tube axis $k_\perp$ are quantized with boundary condition $j \cdot \lambda = |\mathbf{C}| = \pi \cdot d$, yielding for $k_\perp$

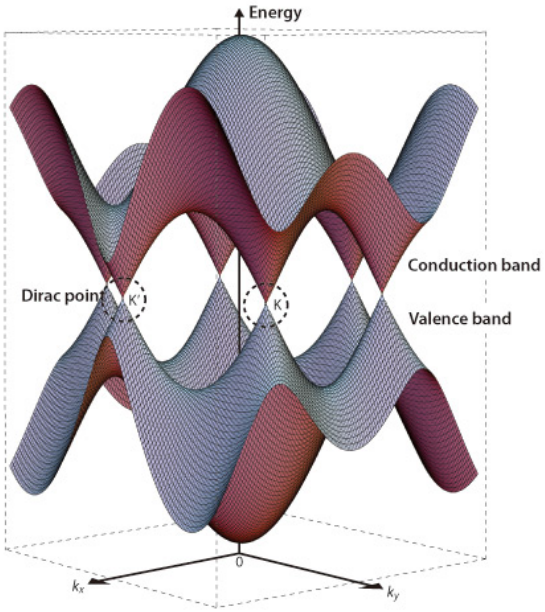

Figure 2.2. Energy dispersion relation for graphene. The six points where valence and conduction band touch are known as Dirac points K and K'. From Ref. [22].

$$k_\perp = \frac{2\pi}{\lambda} = \frac{2\pi}{|\mathbf{C}|} \cdot j = \frac{2}{d} \cdot j \tag{2.3}$$

with integer j.[21] This means the dispersion relation for carbon nanotubes is given by a set of one dimensional subbands. Figure 2.3 shows the contour plot of the graphene band structure with a superimposed Brillouin zone of a metallic carbon nanotube (left) and a semiconducting nanotube (right). The allowed states fall into a series of subbands, depicted as dashed lines. The spacing of the subbands is dictated by the diameter of the nanotube, while the tilt with respect to k_x is determined by the chiral angle. Figure 2.3 a gives the Brillouin zone of a metallic carbon nanotube: The K points are allowed states, i. e., lie on the subbands. Analogously, none of the subbands in Fig. 2.3 b contain a K point, consequently, there is no allowed state at the Fermi energy, indicating that the corresponding nanotube is semiconducting. Every carbon nanotube has a unique set of subbands with respect to the graphene dispersion relation. These subbands follow directly from the nanotube morphology described by the chiral vector (n, m).

The electronic density of states is strongly dependent on the dimensionality of a given system. A one-dimensional system like a nanotube exhibits a $1/\sqrt{E}$ behavior for every subband; the peaked DOS is called van-Hove singularity. A derivation of the precise analytical expression can be found, for instance, in Ref. [21]. The density of states

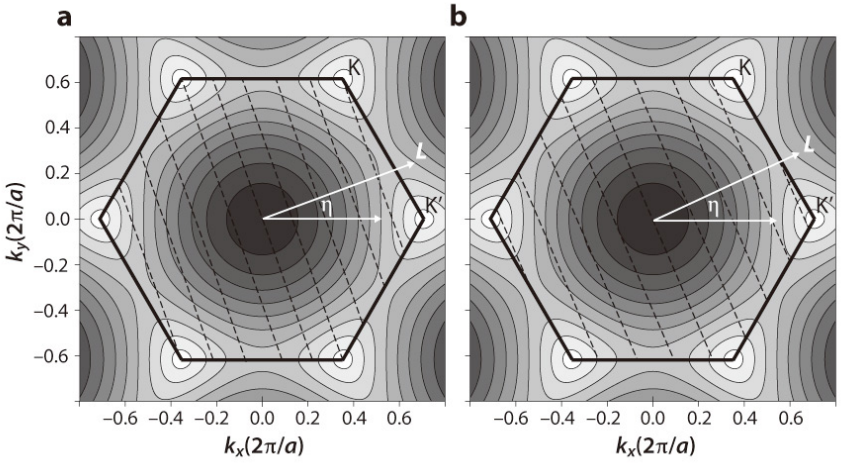

Figure 2.3. Contour plot of the electronic structure of graphene with superimposed nanotube Brillouin zones (dashed lines). (a) shows the band structure of a metallic nanotube; note how the K points lie on the subbands. The band structure in (b) belongs to a semiconducting nanotube, none of the K points is an allowed state. From Ref. [22].

obtained for semiconducting tubes is shown in Fig. 2.4.

Selection rules dictate the optically allowed transitions. Photons polarized parallely to the tube axis can effect transitions between subbands with equal indices, i. e., lift an electron from the ith valence to the ith conduction band. The energies of these transitions are then called E_{ii}. Light polarized perpendicularly to the tube axis has to result in a subband change of one, for instance lifting an electron from the second valence to the first conduction band; the corresponding transition energy is E_{21}. These transverse transitions are highly suppressed due to a strong depolarization by the nanotube, the so-called antenna effect.[24] Consequently, the dominant optical transitions are those between subbands of the same index.

2.1.2. Excitonic effects

Initially, optical transitions in nanotubes were construed as band-to-band transitions. The experimental transition energies were much smaller than the theoretically predicted ones, but correct chirality assignments were made based on the pattern of transition energies of different chiralities.[25] This discrepancy disappeared once many-body effects were taken into account. Ab initio calculations pointed towards binding energies on the order of several 100 meV for dark and bright excitons,[26; 27] which were experimentally confirmed in two-photon absorption measurements.[28; 29]

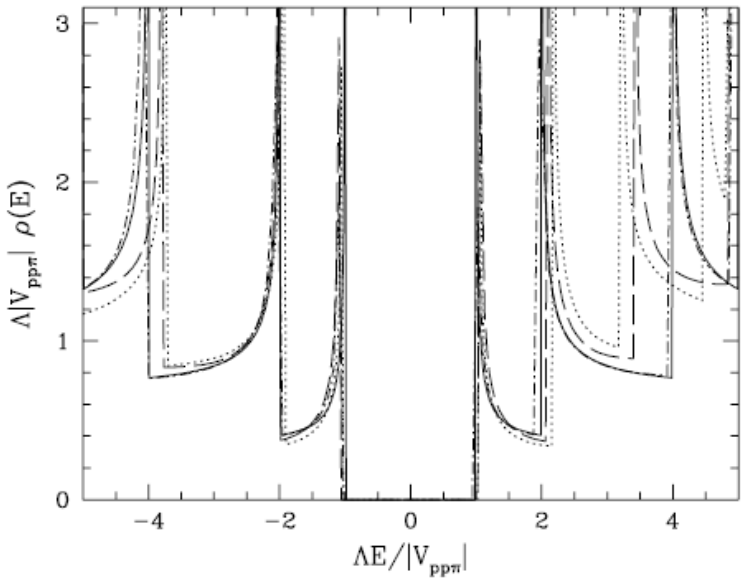

Figure 2.4. DOS calculated for a generic semiconducting nanotube (full line), and three semiconducting nanotubes (dashed, dotted, dash-dotted) with an ab-initio ansatz. All energies and densities were scaled with a dimensionless parameter accounting for the diameter of the tube. From Ref. [23].

Contributions to the energy difference between the single-particle and the many-body picture stem primarily from the electron-electron interaction, which increases the transition energies, and the Coulomb interaction between the electron and the hole, which decreases the exciton's energy. Accounting for both effects, the transition energies are reduced by several 100 meV compared to the band-to-band transitions. For a detailed review see Ref [30]. For every transition, the corresponding bands in the single-particle picture become excitonic bands with additional selection rules, detailed below. The single-particle states still exist, however, they lose importance because the oscillator strength shifts towards the strongly bound optically allowed excitonic states. The single-particle states are commonly referred to as the continuum states.

In nanotubes, the lowest lying state in the single particle bands is four-fold degenerate, once with respect to spin, and once with respect to valley (K or K'). This degeneracy is lifted in the excitonic picture:[31] the lowest energy exciton is a symmetric linear combination of an electron and a hole from the same valley with the same spin and has thus zero circumferential angular momentum. Because of the even symmetry of its wavefunction, it cannot couple to light. The energetically second lowest exciton is also comprised of an electron and a hole from the same valley, but with opposite spins. These

excitons are optically bright. The two other excitons consist of electrons and holes from different valleys and are thus also dark.

Consequently, in single photon spectroscopy we see the lowest lying bright exciton instead of the actual band-to-band transition. In the remainder of this manuscript the transitions introduced above as E_{11}, E_{22}, and so on, will refer to these excitonic transitions, not the band-to-band transitions.

2.1.3. Photoluminescence of nanotubes

Photoluminescence in carbon nanotubes was first reported in 2002[32] and quickly became one of the primary tools for identifying the chirality of single semiconducting nanotubes, and characterizing the chirality distribution of polydisperse nanotube samples. The reason it took a decade from the discovery of single walled nanotubes to the first observation of their luminescence is that nanotubes bundle strongly owing to their extended π-orbitals. In bundles, excitons created in semiconducting nanotubes can transit into metallic nanotubes, where they recombine non-radiatively. Consequently, photoluminescence in nanotube bundles is quenched. With time, protocols for efficient nanotube dispersion and individualization were devised, typically involving one or several surfactants, ultrasonication, and centrifugation.

The photoluminescence process in semiconducting carbon nanotubes involves three steps. Radiative excitation at one of the transition energies (E_{11}, E_{22}, E_{33}, $\cdots$) induces an electron-hole pair in the corresponding excitonic band. Subsequently, intersubband relaxation takes place, both electron and hole relax non-radiatively to the lowest excited states, E_{11}, from where radiative recombination takes place, see Fig 2.5.

The time scale of the photoluminescence is still under debate, as both the tube's dielectric environment as well as defects reduce lifetimes considerably. Generally agreed upon is the intersubband relaxation. At low excitation densities, i. e., at excitation densities in which the PL intensity dependence on pump fluence is linear, intersubband recombination was reported to occur on a time scale of several 10 fs. Two color pump-probe experiments yield relaxation times around 40 fs for the relaxation from E_{22} to E_{11} and 65 fs from E_{33} to E_{11}.[33] The radiative lifetime on the other hand is highly sensitive on the tube's environment. Calculations for room temperature tubes in vacuum result in radiative life times on the order of tens of ns.[34; 35] In experimental reports the photoluminescence decay takes place in tens of ps. However, once non-radiative recombination rates as extracted from measurements of quantum yield are taken into account, these results diverge widely, resulting in radiative lifetimes between 10 ns and 3 μs.[36; 37] Ultimately, the quantum yield, and with it the photoluminescence decay,

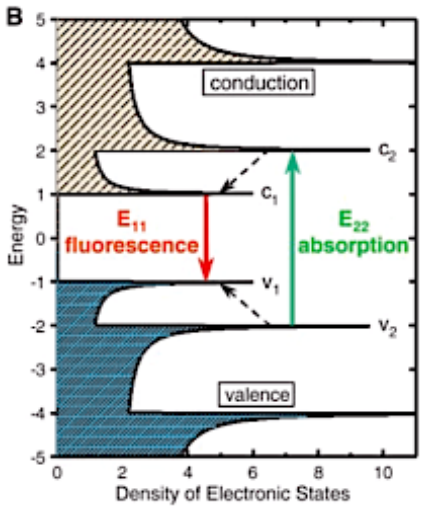

Figure 2.5. Photoluminescence process in semiconducting carbon nanotubes: Excitation at the E_{22} transition energy is followed by non-radiative relaxation into the E_{11} state, from which the radiative recombination occurs. From Ref. [25].

strongly depends on the preparation conditions of the nanotube: Excitons in a one dimensional system are in effect unshielded against environmental influences. Quantum yields as high as 7% have been achieved for long suspended nanotubes, while typical values for surfactant suspended tubes in aqueous solution are below 0.1%.[38]

A widely used tool in nanotube PL spectroscopy is the photoluminescence excitation map, see Fig. 2.6. By measuring the photoluminescence emission for a range of excitation energies, a 3D map is formed. In a PLE map, the y-axis corresponds to the excitation wavelengths and the x-axis to the emission wavelengths. Consequently, every peak in the white ellipse in Fig. 2.6 corresponds to the E_{22} excitation energy and the E_{11} emission energy of a particular chirality.

E_{11} and E_{22} are given by

$$\begin{aligned} E_{11} &= \frac{2\gamma_0 a_0}{d} + (-1)^\nu \frac{t_{11}\cos 3\theta}{d^2} \\ E_{22} &= \frac{4\gamma_0^* a_0}{d} - (-1)^\nu \frac{t_{22}\cos 3\theta}{d^2}, \end{aligned} \tag{2.4}$$

where a_0 is the lattice constant, d is the nanotube diameter, θ is the chiral angle, ν is given by $n - m \pmod 3$, and γ_0, γ_0^*, t_{11}, and t_{22} are parameters.[38] Plotting these data against the inverse diameter $1/d$ yields the so-called Kataura plot, Fig. 2.7. For every

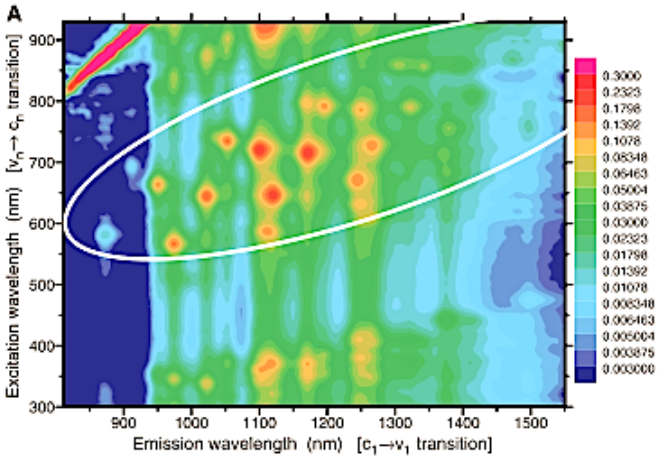

Figure 2.6. Photoluminescence excitation map for a polydisperse carbon nanotube sample. Excitation wavelengths are on the y-axis, emission wavelengths on the x-axis. Every peak is characterized by a unique combination of E_{11} and E_{22} transition energies, corresponding to a certain nanotube chirality. From Ref. [25].

transition E_{11}, E_{22}, ... a clear $1/d$ dependence is evident, as dictated by the first terms in Eq. (2.4). From this linear relationship branches emanate, tilting to lower and higher transition energies. This deviation from the linear relationship stems from the second terms in Eq. (2.4), which are owed to the so-called trigonal warping effect.[39] Depending on $\nu = n - m \pmod 3$, excitonic energies are either lower or higher than indicated by the linear relationship in $1/d$. For the $\nu = 1$ family, exciton energies are lower for E_{11} and higher for E_{22}. For $\nu = 2$, this behavior is exactly reversed. Near-armchair tubes follow the linear $1/d$ relationship closely, while near-zigzag tubes lie at the ends of the branches. Whether the branch tilts towards lower or higher energies depends on which side of the K point the subband cuts the graphene Brillouin zone, between K and Γ point, or between K and M point.

PLE maps are widely used to characterize the chirality distribution of nanotube samples. To this end, PL spectroscopy is a very convenient and powerful tool, however, it harbors several pitfalls. First, metallic nanotubes cannot be accounted for since they do not exhibit luminescence. To map metallic tubes one has to resort to Raman spectroscopy. Secondly, the light coupling strength depends on the chirality, so while one can compare the intensity of a particular chirality across different samples, comparing PL emission intensities of different chiralities to one another is much more difficult. Lastly, the luminescence intensity is highly sensitive to the bundling state of carbon nanotubes. Bundled nanotubes do not exhibit luminescence because typically faster non-radiative

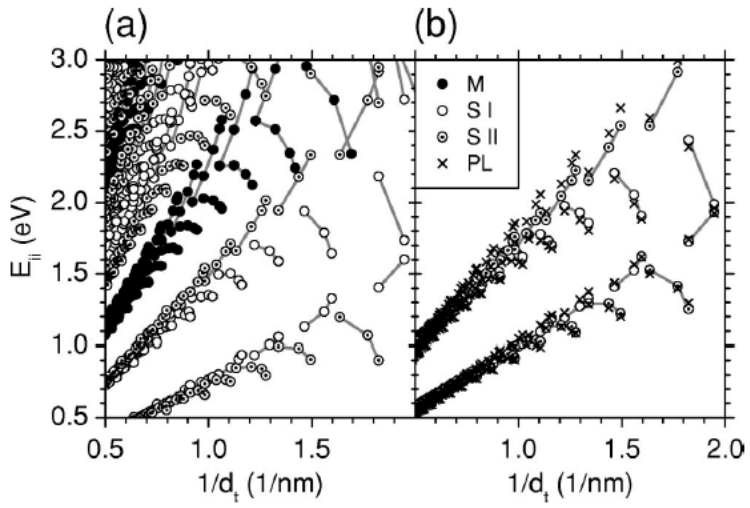

Figure 2.7. Kataura plot of the transition energies E_{11}, E_{22}, ... against $1/d$. Semiconducting chiralities with $\nu = 1$ are given by open circles, semiconducting chiralities with $\nu = 2$ are given by dotted circles, metallic tubes by full circles. Results in (a) are calculated by tight binding in the single particle picture. (b) takes many-body effects into account, and matches the experimental data (crosses) well. From Ref. [40].

recombination pathways exist for excitons. It has been demonstrated that the bundling prevalence differs between different chiralities, resulting in a disproportionate PL intensity distribution.[41]

2.1.4. Chirality separation

In effect, different nanotube chiralities are different materials with distinct optoelectronic properties. Many of the countless applications nanotubes have been suggested for crucially hinge on the procurement of single chirality samples. In principle, there are two ways of approaching this problem, monochiral growth and ex-post separation. Despite extensive efforts to attain chirality selective growth, resounding success remains elusive. Currently, nanotube growth can be restricted to a reasonably narrow diameter range, however, tubes of very similar diameter can have highly disparate optoelectronic properties, see Sec. 2.1.1.

Post-growth separation is at present the only viable road to monochiral samples. Nanotube sorting is a large and very active field of research with a sizable range of approaches; we will give a very brief overview, for an extensive review see Ref. [42].

The first approach for nanotube sorting was selective chemistry. Reactivity with diazonium salts depends on the number of electrons near the Fermi energy E_F, resulting in selective functionalization of metallic nanotubes. By ionizing the covalently attached

salt, metallic and semiconducting tubes can then be separated through electrophoresis.[43] Tubes can also be separated into their electronic type through a gel squeezing based method. This approach relies on the selective interaction of metallic tubes with the gel.[44; 45; 46] Dielectrophoresis and selective destruction are also used for separation by electronic type only. Density gradient ultracentrifugation allows sorting nanotubes not only by electronic type but by their buoyant density in micellar suspension.[47]

Several surfactants display chiral preferences. Solubilization through polymers with varying aromatic moieties results in differences in the chirality distributions as observed in PLE maps.[48; 49] Similar results have been reported with large biomolecules: some oligonucleotide patterns in single stranded DNA solubilize certain nanotube chiralities preferentially.[50; 51; 52] These interactions are generally attributed to the characteristic spatial pattern of the extended π orbital network along the nanotube axis. This pattern depends on the chiral vector (n, m), i. e., the chirality. Small surfactants containing aromatic moieties can also change the photoluminescence intensity distribution across different chiralities.[53; 54; 55; 56]

While some progress has undoubtedly been made in advancing nanotube chirality separation, none of the current methods are satisfactory in terms of throughput or scalability. Especially DNA based methods as well as large column chromatography hold promise, for the moment the problem of nanotube sorting very much remains.

2.2. Energy transfer systems

Energy transfer systems in their basic form consist of two subsystems, the designated donor **D** and the designated acceptor **A**, with respective absorption and emission spectra $f(\lambda)_D^{abs}$, $f(\lambda)_D^{em}$, and $f(\lambda)_A^{abs}$, $f(\lambda)_A^{em}$. For energy transfer to be possible, the emission spectrum of the donor $f(\lambda)_D^{em}$ has to possess a spectral overlap with the absorption spectrum of the acceptor, $f(\lambda)_A^{abs}$, see Fig 2.8. When the donor system **D** is brought into an excited state, usually through radiative excitation, there is a probability that this excitation is subsequently transferred into the acceptor system **A**. Consequently, the spectroscopic signature of energy transfer is (i) a quenching of the donor's own emission, and (ii) emission of the acceptor **A** after excitation of the donor **D**.

There are two types of fluorescence energy transfer, Förster resonance and Dexter energy transfer.[57] The Förster resonance energy transfer stems from the coupling of dipoles: The exciton in the donor induces a mirror dipole in the acceptor. The two dipoles then couple together, resulting in a finite probability for non-radiative energy transfer. The other possible mechanism, the Dexter energy transfer, involves the physical exchange

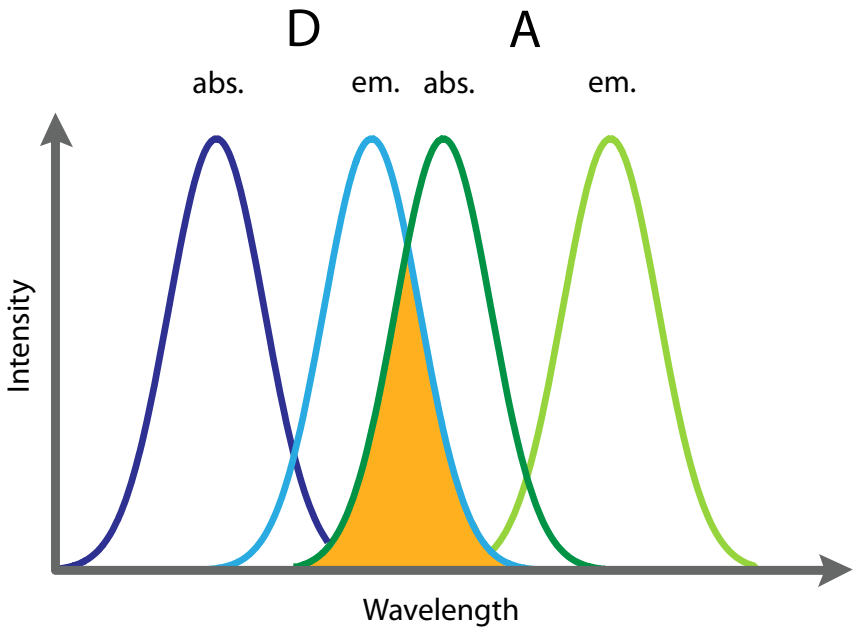

Figure 2.8. Absorption and emission spectra of the donor **D** (blue) and the acceptor **A** (green). For energy transfer to be possible, the emission of the donor and the absorption of the acceptor have to spectrally overlap. The overlap is marked in orange.

of two electrons. An excited electron is passed from the donor **D** to the acceptor **A**, while a ground state electron is passed from the acceptor to the donor. Both processes are schematically depicted in Fig. 2.9. For spin singlet systems the two processes cannot be distinguished by their outcomes. Energy transfer in spin triplet systems is only possible when the electrons are physically exchanged, i. e., in the Dexter transfer.

The transfer efficiency for both processes crucially depends on the distance between donor and acceptor. For Dexter energy transfer the distance range is restricted by the necessity of electron orbital overlap, with typical exchange distances below 1 nm. Because the Dexter process requires a double electron transfer, the transfer rate is much lower than for the Förster transfer. For triplet-triplet transfer systems the Förster coupling is forbidden, and the Dexter transfer becomes the dominant mechanism. The Förster resonance is a dipole interaction, and thus has a much larger range of up to several 10 nm. The transfer efficiencies of almost unity achieved in nanotube-chromophore complexes indicate that the relevant transfer mechanism here is the Förster resonance, see Section 2.3.

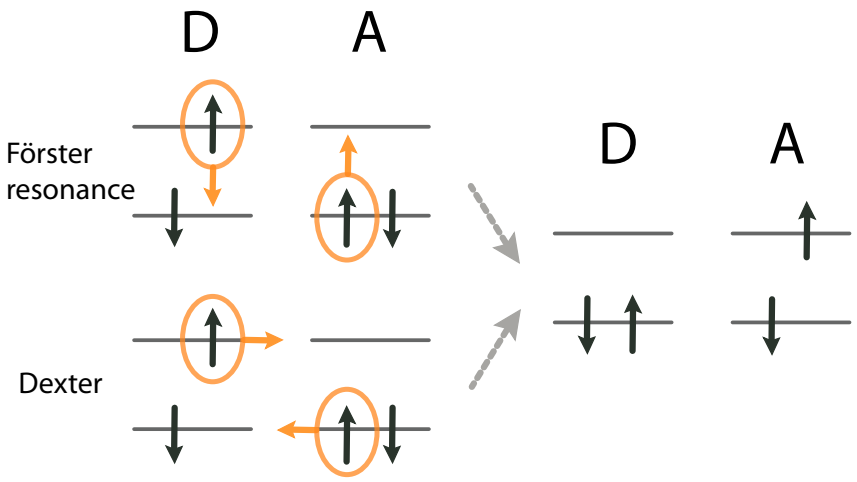

Figure 2.9. Fluorescence energy transfer comes in two flavors. Förster resonance (top) is based on dipole-dipole coupling between donor **D** and acceptor **A**, while the Dexter transfer (bottom) involves a double electron transfer. An excited electron is passed from donor **D** to acceptor **A**, while a ground state electron is passed back. For spin singlet systems the result is identical for both mechanisms.

2.2.1. Förster resonance energy transfer

Dipole mediated energy transfer was first observed and recognized as such in 1922 in a thallium mercury vapor mixture. A quantitative description was formulated in the second half of the 1940s by Theodor Förster. For a short historical review of the Förster process see Ref. [58].

A system with a Förster-like coupling is completely characterized by one parameter, the Förster radius R_0. R_0 is defined as the distance between the two subsystems at which half of the excitations created in the donor are transferred into the acceptor, and half decay in the donor itself. The Förster radius can be derived quasi-classically: The dipole-dipole term of the multipole expansion of the Coulombic interaction between two charge densities is considered in a point-dipole approximation, yielding for R_0

$$R_0 = \left[\Phi_D \cdot \frac{9c\kappa^2}{64\pi^2 n^4} \int_0^\infty f_D(\lambda) f_A(\lambda) \lambda^2 \mathrm{d}\lambda \right]^{1/6}, \tag{2.5}$$

with $f_D(\lambda)$ the normalized emission spectrum of the donor and $f_A(\lambda)$ the normalized absorption spectrum of the acceptor, Φ_D the fluorescence quantum yield of the donor, n the refractive index of the medium, c the speed of light, and where $\kappa^2 = [0...4]$ is a parameter specifying the relative orientation of the dipoles. For unknown orientations

the orientational average is used, $\kappa^2 = 2/3$. Using Eq. (2.5), the Förster radius R_0 can be calculated for any energy transfer system for which the emission spectrum of the donor $f_D(\lambda)$ and the absorbance spectrum of the acceptor $f_A(\lambda)$ are known.

The efficiency of the energy transfer E is given by $E = 1 - F_D^A/F_D$, where F_D^A is the fluorescence emission of the donor in the presence and F_D the fluorescence emission of the donor in the absence of acceptor **A**, respectively. Hence, F_D^A/F_D is the fluorescence quenching of the donor **D** in the presence of the acceptor **A**. The transfer efficiency E is experimentally easily accessible and in conjunction with the analytically calculated R_0 yields the distance R between the donor **D** and the acceptor **A**

$$R = R_0 \cdot \sqrt[6]{\frac{1}{E} - 1} = R_0 \cdot \sqrt[6]{\frac{F_D^A}{F_D}}. \tag{2.6}$$

Hence, the experimentally measured transfer efficiency can be used as a molecular ruler in conjunction with the analytically calculated Förster radius R_0 of the system.

2.3. Carbon nanotube - chromophore energy transfer systems

Energy transfer complexes can be created from nanotubes and chromophores. Many chromophores emit in the visible, where semiconducting nanotubes absorb light: The E_{22} of HiPco nanotubes typically range between 500-800 nm depending on chirality, see the photoluminescence excitation map in Fig. 2.6. So, in principle, chromophores with an appropriate emission resulting in a spectral overlap with the absorption of the nanotubes are suitable for nanotube-chromophore energy transfer complexes, see Fig. 2.10. While the HOMO and LUMO levels of molecules are typically depicted as discrete energy levels, they generally are not spectrally sharp, owing to vibrational states. This is seen in typical absorbance and luminescence spectra of dyes. Both absorbance and emission typically range over many 100 meV. Consequently, it is possible to choose a chromophoric unit for which the emission spectrum overlaps with all E_{22} energies in a typical nanotube sample. This is a very general idea, and the actual creation of the energy transfer complexes is a highly non-trivial task. As seen in Sec. 2.2, the energy transfer efficiency depends on the distance in the sixth power, making a close spatial proximity between the dye as excitation donor and the nanotube as excitation acceptor paramount.

Energy transfer from a chromophore into carbon nanotubes was first observed by Qu *et al.* in 2002.[59] Nanotubes were covalently functionalized with pyrene derivatives, whereupon the fluorescence, not, however, the absorbance, of the pyrene was quenched, a

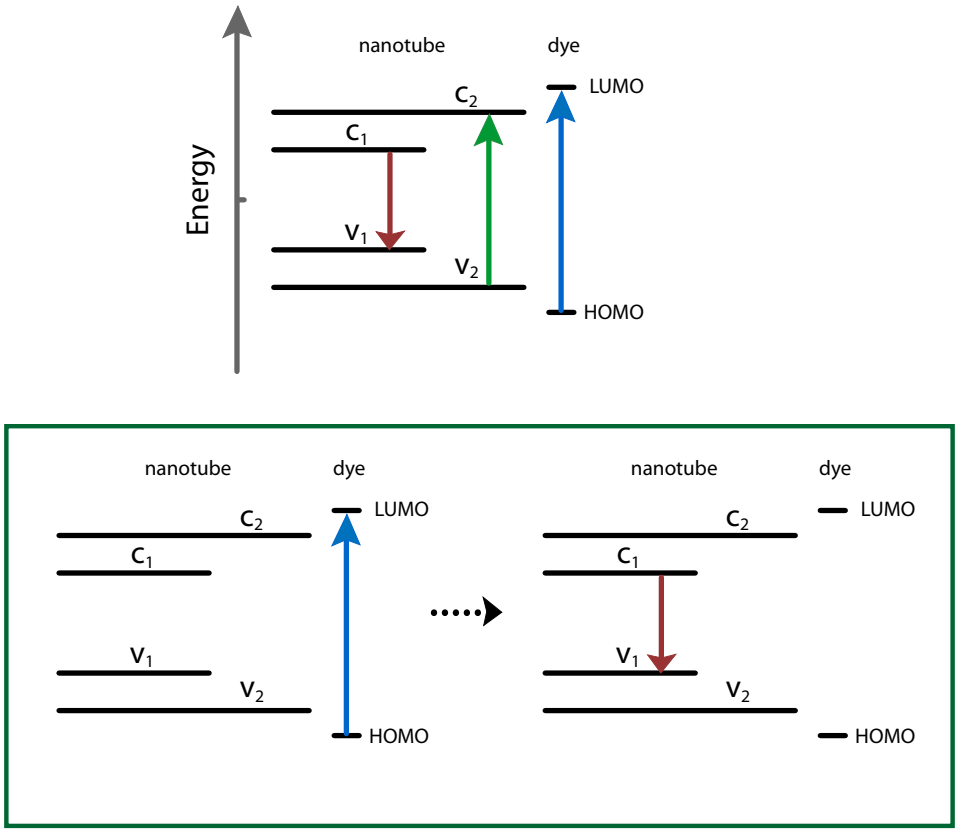

Figure 2.10. Schematic diagram of the lineup of the band structure of a semiconducting carbon nanotube with the HOMO and LUMO of a dye. The HOMO-LUMO gap of the dye has to be the same size as one of the resonant transitions in the nanotube. The resonant transitions of the nanotube are energetically narrow, but typical dye emissions are broad due to vibrational states. In the lower panel the anticipated result is illustrated: After the excitation of the dye the exciton is passed into the nanotube. In the nanotube the exciton relaxes to the E_{11} ground state, from where it can radiatively recombine.

strong indication for energy transfer. The subsequent luminescence emission of the nanotubes was not observed. For one, photoluminescence from nanotubes had only just been observed a couple of months earlier for the first time,[32] and covalent functionalization strongly quenches the nanotube luminescence due to the introduction of defects in the sp^2 bonded carbon network which serve as non-radiative recombination sites, see Sec. 2.1.3. However, this means other mechanisms for the pyrene luminescence quenching could not be completely ruled out. For instance, the spatial ordering of the pyrene derivative molecules on the carbon nanotube may have led to self-quenching.

The first time that energy transfer from a chromophore was demonstrated unambiguously was in 2005 by Feng *et al.* [60] in multiwall nanotubes which were non-covalently functionalized through π-π stacking with perylene derivatives. Multiwall nanotubes, just like bundles and covalently functionalized tubes, do not exhibit any photoluminescence, see Sec. 2.1.3. However, after excitation of the perylene derivatives a jump in the photocurrent of the nanotubes was observed, a testament to additional electron-hole pairs stemming from the perylene.

Spectroscopic observation of the NT luminescence in the infrared after excitation of the chromophore was reported two years later by Yanagi *et al.*[61] In their study squarylium dye was inserted into the nanotube. Upon excitation of dye an emission from the nanotube was observed, see Fig. 2.11. Nish *et al.* reported similar results in 2008 for polymer-wrapped nanotubes.[62]

Aside from endohedral and polymer functionalization two other methods of creating nanotube-chromophore energy transfer complexes have been demonstrated. First, the incorporation of chromophoric units into surfactants, the subject of this thesis. [9; 10; 55; 56; 63] Nanotubes are strongly hydrophobic and are typically dispersed with the help of surfactants in a ultrasonication and centrifugation procedure. The incorporation of the chromophore, in this case a perylene derivative, into the surfactant ensures spatial proximity and temporal stability. The PLE maps in Fig. 2.12 show a sodium cholate (SC) suspended HiPco sample on the left and the same sample suspended with a functional surfactant, **C16**, entailing a perylene derivative unit. All peaks above the gray line are the E_{22} excitation/ E_{11} emission peaks and are seen in both SC and **C16** samples. The peaks below the gray line correspond to the E_{11} emission of the nanotubes after an excitation of the **C16** surfactant. On the right in Fig. 2.12 we show the luminescence of **C16** before (top) and after (bottom) complexation with nanotubes. The luminescence is quenched by a factor of up to 10^4.[9] The precise design of the tailored surfactant turned out to be of great importance for both qualities as a surfactant and for the energy transfer capabilities. Of ten tailored surfactants five formed energy transfer complexes.[63] The suitability as a

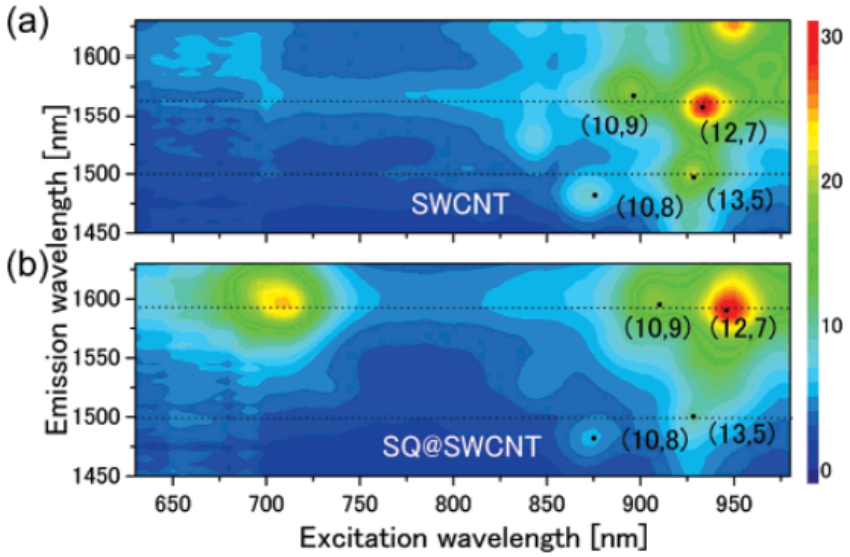

Figure 2.11. PLE map of nanotubes before (a) and after (b) insertion of squarylium dye into the carbon nanotubes. Note the nanotube emission after excitations ∼700 nm after insertion of the dye. This is the nanotube luminescence after excitation energy transfer from the dye. From Ref. [61].

surfactant also varied, see Fig. 2.13, which shows stylized surfactant symbols ranked by nanotube solubilization and individualization quality, Fig. 2.13 a. We show the number of suspended bundles vs. the photoluminescence intensity per tube, a measure for the amount of individualized tubes, see Sec. 2.1.3. In Fig. 2.13 b the same data on the y-axis are plotted against alkyl chain lengths (alkyl chains are depicted in green), indicating that there is an ideal length for the alkyl chains in a tailored functional surfactant. Including the chromophoric unit into a functional surfactant has proved to be a temporally stable and highly efficient way of forming energy transfer complexes.

The other route is the functionalization via micelle swelling. In 2008 it was reported that organic solvents can enter the micelles of bile salt suspended nanotubes in water.[64] Dichlorobenzene (DCB), a water immiscible organic solvent, was stirred into a solution of sodium dodecyl sulfate (SDS) and sodium dodecylbenzene sulfonate (SDBS) suspended tubes. Spectroscopically, three effects were observed. (i) The luminescence of the nanotubes was temporarily quenched, but recovered gradually after many hours to the original level. This was rationalized by the organic immiscible solvent entering the nanotube micelles, which are unpolar on the inside. In the micelle, they perturb the dielectric environment of the nanotube, resulting in increased non-radiative recombination.

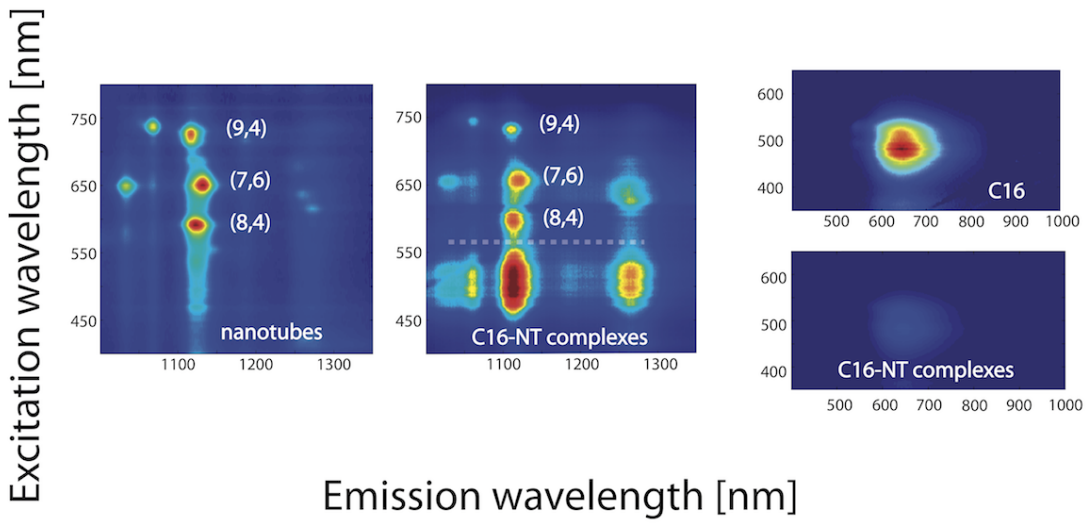

Figure 2.12. PLE maps of a SC suspended HiPco sample (left) and a **C16** suspended sample (middle). Note that the E_{22} excitation/ E_{11} emission peaks and are seen above the gray line in both samples. The peaks below the gray line in the **C16** sample correspond to the E_{11} emission of the nanotubes after excitation of the dye in the **C16** molecule. The **C16** luminescence is shown on the right before (top) and after (bottom) complexation with nanotubes. It is quenched by up to 10^4.

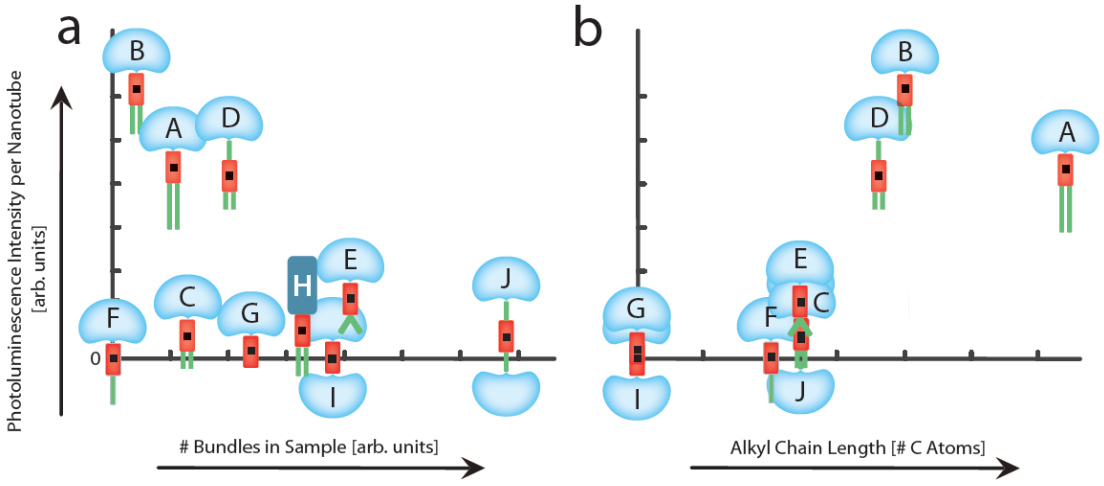

Figure 2.13. Ten functional surfactants are ranked by the quality of their solubilization and individualization of nanotubes. In panel a the number of bundles in the sample is plotted agains the PL intensity per tube. High values for the PL intensity correspond to good individualization. In panel b the same PL intensity data are shown against the alkly chain lengths, alkyl chains are depicted in green. From Ref. [63].

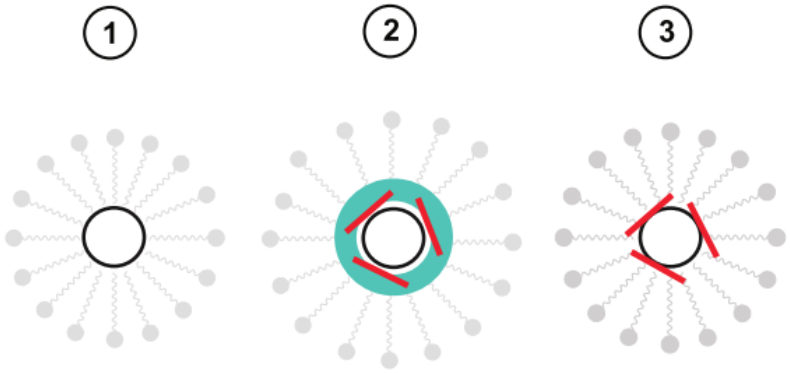

Figure 2.14. Diagrammatic depiction of the chromophoric insertion into a surfactant suspended micelle via swelling of the micelle. Both organic solvent (green) and chromophore (red) are introduced into the micelle surrounding the nanotube, but only the solvent evaporates subseqently, resulting in micelle suspended nanotube-chromophore complexes. From Ref. [65]

Eventually, the DCB evaporates and the luminescence recovers fully. (ii) Together with the quenching, a shift in the luminescence peaks is observed. This points to a different dielectric environment caused by DCB inside the micelles. (iii) The luminescence of some chiralities was permanently enhanced. This indicates that the micelles reorganize around the nanotubes such that certain preferentially bundling chiralities are separated more efficiently, leading to increased luminescence, see Sec. 2.1.3.

Roquelet *et al.* used the micelle swelling technique with organic chromophores as a vehicle for introducing chromophores into the micelles.[65; 66; 67; 68] Organic chromophores are typically soluble in organic media, i. e., in DCB but not in water. By mixing the chromophores in volatile organic media into aqueous solutions of bile salt suspended nanotubes, both solvent and chromophores are introduced into the nanotube micelles, see Fig. 2.14. The solvent gradually evaporates out of the micelle, leaving the nanotube-chromophore complexes behind in the micelle. This approach is more flexible than the tailored design of functional surfactants, but is also less robust. Additionally, some chromophores do not lend themselves to micelle swelling, see Sec. A.1.

3 | Connection of the papers

Endohedral functionalization of carbon nanotubes with squarilium dye yielding energy transfer complexes was reported from the Kataura group in Tokyo in 2007,[61] and first successes in the functionalization with polymers resulting in energy transfer into tubes were achieved by the group around Nichols in Oxford the following year.[62] When I set out on this project in 2010, energy transfer between chromophores and structurally intact single wall nanotubes had not been demonstrated for non-covalent functionalization with single molecules. Simultaneously with this work, the Lauret and Voisin groups in Paris developed the micelle swelling technique, which is covered in Sec. 2.3.[65; 66; 67; 68] Figure 3.1 shows all three routes to creating energy transfer complexes: (A) exohedral non-covalent functionalization with small molecules (B) polymer wrapping, and (C) endohedral functionalization.

Our approach to this problem was the incorporation of a dye unit into a surfactant molecule. The surfactant would then both solubilize the tubes in water, and at the same time form energy transfer complexes with the tube. This tailored surfactant had to entail three functional units: A hydrophilic part for water solubility, a hydrophobic part for the interaction with the nanotubes, and the chromophore itself, see Fig. 3.2. We opted for perylene derivatives, mostly perylene diimides, as the chromophoric unit. This choice

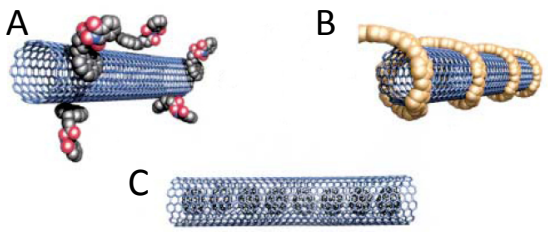

Figure 3.1. Functionalization of nanotubes: (A) Exohedral non-covalent functionalization with small molecules, (B) polymer-wrapping of nanotubes, (C) endohedral functionalization. Adapted from Ref. [69].

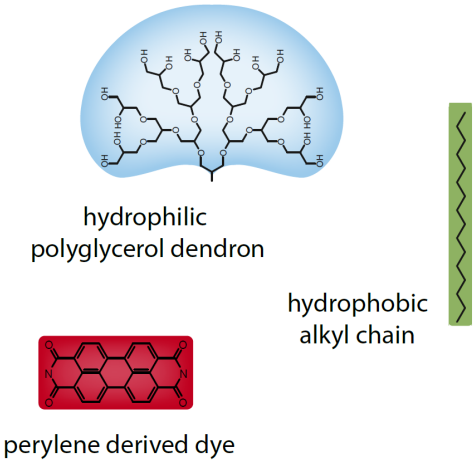

Figure 3.2. Functional units for the assembly of the energy transfer surfactant. A perylene derived dye (red) is responsible for the energy transfer capability. Water solubility is afforded by the hydrophilic polyglycerol dendron (blue), and the interaction with the nanotubes is mediated by the alkyl chains (green).

was made for several reasons. As detailed in Sec 2.3, the emission spectrum of the donor **D** has to overlap with the absorption spectrum of the acceptor **A**, here the nanotubes. The nanotube E_{22} transition energies for HiPco samples lie around 550 nm-780 nm, which matches the emission of the perylene derivatives. Furthermore, the perylenes absorb from 450 nm-520 nm, a spectral region without resonant nanotube transitions. Consequently, if an excitation in the chromophore absorption band is followed by an emission at an energy characteristic of nanotube E_{11} energies in the NIR, we can be sure that energy transfer has occurred. Additionally, perylene has a luminescence quantum yield of 0.99, and possesses extended π orbitals which can interact with the nanotube's π orbitals for efficient stacking.[8; 70]

For the hydrophilic part of the tailored surfactant we chose a polyglycerol dendron; this constituted an unusual choice because PG dendrons are difficult to synthesize. Most surfactants utilize a charged or dipolar headgroup (including all bile salt surfactants) or non-ionic polyethylene glycol (PEG) instead. PEG is similar to PG dendrons, however, it is a linear chain molecule, lacking the tree-like characteristic of the dendron, see Fig. 3.2. PG dendrons are well known for their ideal biocompatibility:[71; 72; 73; 74; 15] Proteins do not stick to PG dendrons, consequently these molecular units are used, for instance, as coatings in anti-fouling surfaces. This low level of interaction with proteins makes them also attractive for biomedical surfactants, since protein function can be impeded by adsorbed contaminants such as nanotubes.

The last unit of the functional surfactant is the hydrophobic alkyl chain, which is found in almost all traditional nanotube surfactants. The chains interact with the nanotube itself, solubilizing and individualizing it.

These three building blocks can be combined in multiple ways, resulting in a family of structurally similar surfactants which we later use to investigate the effects of design on surfactant function. The first molecule that we developed which both solubilized nanotubes and formed energy transfer complexes is shown in Fig. 3.3. The resultant photoluminescence measurements of the energy transfer complexes are shown in Fig. 2.12. The left and middle panels respectively show luminescence maps for HiPco nanotubes solubilized with SC and the perylene based energy transfer surfactant. All peaks below the gray line correspond to the E_{11} emission of the nanotubes after an excitation through the absorption band of the perylene. Consequently, they are only observed in the perylene surfactant solubilized sample. All peaks above the gray line correspond to the E_{11} emission of the nanotubes after an excitation at the E_{22} energies of the corresponding chiralities and are seen in both samples. Fig. 2.12, right, shows the luminescence of the functional surfactant itself before (top) and after (bottom) complexation to the nanotubes. The quenching of the perylene luminescence emission in the presence of nanotubes is evident.

The main challenge that had to be overcome for solubilizing nanotubes with the functional perylene based surfactant consisted in finding the right parameters for the solubilization process. Perylene possesses a hot luminescence in the near infrared. Consequently, if too much surfactant is used, the free perylene surfactant masks the energy transfer signal. On the other hand, when too little surfactant is used, the nanotubes remain bundled and the degree of nanotube individualization is not sufficient for observing photoluminescence, see Sec. 2.1.3. The protracted process of determining the right processing parameters is detailed in section A.1.1.

Fortunately, once a good sample preparation protocol was devised, the molecule's solubilization behavior emerged as superb. The interaction strength between nanotube and perylene based surfactant is unusually large owing to the intimate π-π stacking mechanism, skewing the dynamic equilibrium between adsorbed and free dye at room temperature heavily in the favor of the adsorbed form. Hence, it is possible to find concentration parameters for which almost all surfactant is adsorbed onto nanotubes, reducing the free perylene's own emission to almost zero. These proof of principle results were published in the first of the papers comprising this thesis, Ernst *et al.*, Adv. Funct. Mater. **22**, 3921-3926 (2012).

We followed up this work by investigating ten structurally similar surfactants to determine the criteria governing (i) whether a molecule is a potent surfactant, efficiently

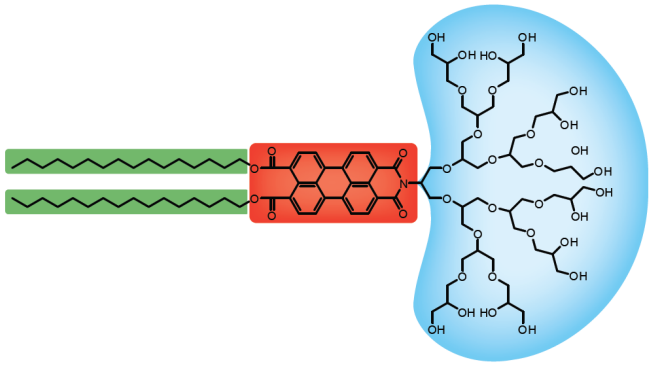

Figure 3.3. First functional surfactant with energy transfer capabilities.

solubilizing and debundling nanotubes, and (ii) whether a surfactant with a chromophoric unit forms energy transfer complexes with the nanotubes. The morphology of ten surfactants was systematically varied and the solubilization and energy transfer behavior assessed. The modularity of this approach allowed us to systematically determine which characteristics are beneficial, and which features best to avoid in the design of functional surfactants. These results are applicable to any kind of functional surfactant for which proximity to the nanotube is paramount.

The assessment of the surfactant capabilities of all ten molecules is shown in Fig. 2.13. Panel a) shows a plot of the number of bundles in the samples against the photoluminescence intensity per nanotube for every surfactant molecule. The photoluminescence intensity per tube is a good measure for the degree of individualization, see also Sec. 2.1.3. We note that the molecules performances as surfactants are diverse. Some surfactants are very good at solubilizing nanotubes, but not at individualizing them. Some other molecules are excellent surfactants with very high luminescence intensities per tube, and three molecules do not interact well with nanotubes at all. The same data on the luminescence intensities per tube are displayed again in Fig. 2.13 b), this time plotted against the total length of all alkyl chains in the molecule. We find a very clear pattern: Longer alkyl chains make for better surfactants, until a maximum total alkyl chain length of 20 carbon atoms is reached. Beyond this length, the surfactant becomes less efficient again, which we attribute to increased desire to form micelles without adsorbing to the nanotubes. Note that the one molecule without the polyglycerol dendron for the hydrophilic unit is not a good surfactant. Instead of the PG dendron the molecule possesses a linear PEG chain. The exact counterpart surfactant with a PG dendron is the best surfactant in our study, demonstrating that the PG dendron is necessary for this type of surfactant design.

The exact morphology of the alkyl chains on the other hand is of little importance for the surfactant's dispersion capabilities.

We also evaluate the surfactants' propensity for forming energy transfer complexes with nanotubes, and find that complexes made with five of the molecules exhibit energy transfer as demonstrated in photoluminescence measurements. However, it is possible that energy transfer also takes place in some, or all, of the other surfactants. Since they do not debundle the nanotubes sufficiently, we cannot resolve a possible energy transfer in luminescence measurements. In conclusion, we recommend for the general design of closely stacking functional surfactants that the functional unit be bound to two parallel alkyl chains with a combined length of 20 carbon atoms on one side, and a PG dendron attached to the surfactant core with an alkyl chain on the other side. The outlined results on the design of functional energy transfer surfactants were published in the second paper of this thesis, Ernst *et al.*, J. Phys. Chem. C **117**, 1157-1162 (2013).

Subsequently, we investigated the energy transfer mechanism in the five energy transfer surfactants. Based on the quenching rate of 10^4 of the donor's emission, we know this is a Förster-type interaction, see Sec. 2.2. The quenching rate in Förster resonance energy transfer only depends on the distance between donor and acceptor, as well as a characteristic distance for the particular donor and acceptor pair, known as the Förster radius R_0. The Förster radius of a system depends on the overlap integral between the donor emission $f(\lambda)_D$ and the acceptor absorption $f(\lambda)_A$, the fluorescence quantum yield of the donor Φ_D, the relative orientation between the dipoles κ^2, the refractive index of the medium n, and the speed of light c. Of these, only κ^2 is unknown. We approximate κ^2 as the orientational average, $\kappa^2 = 2/3$, and are then able to calculate the Förster radius R_0 of the perylene unit with the nanotubes. Since the different chiralities have different E_{22} transition energies, the spectral overlap integral varies for different tubes slightly, yiedling $R_0 = 5.3\,\text{nm}$-$6.6\,\text{nm}$. From the quenching rate we can now determine the actual distance between tube and chromophore, namely $1.2\,\text{nm}$-$1.5\,\text{nm}$.

Subtracting the radius of the tube from this distance, the result is on the order of the van-der-Waals distance of $0.34\,\text{nm}$ for graphitic systems, indicating close stacking between chromophore and tube. We further analyze the excitation channels of all complexes. Surprisingly, the excitation characteristics vary for the different complexes: The five surfactants fall into two groups which differ in the spectral form of their luminescence excitation spectra as well as their excitation transfer rates. The PLE spectra of all five molecules and complexes are shown in Fig. 3.4. The first group comprises three closely stacking molecules. The molecules in the second group stack even more closely as indicated by a 40% higher transfer rate into the nanotube, accompanied by a change in

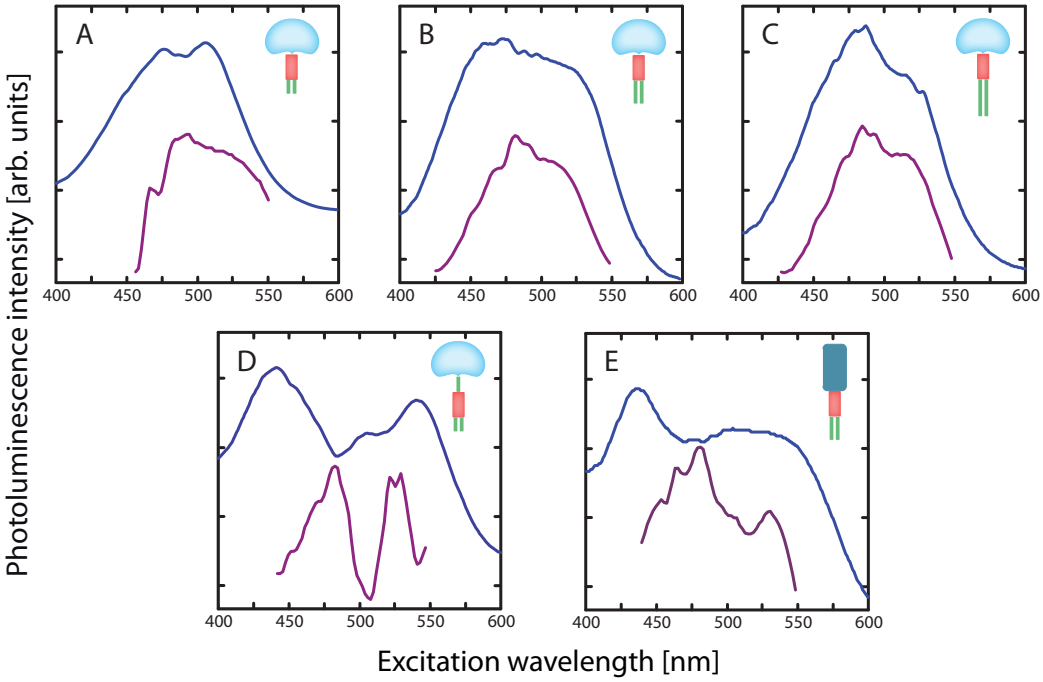

Figure 3.4. Photoluminescence excitation spectra of the indicated molecules alone (blue) and the nanotube-molecule complexes (purple). The PLE spectra for molecules and complexes are similar to each other for the three surfactants in the first line. For the two molecules in the second line, they are different from each other in a similar way, indicating a change in stacking on the tube.

the spectral form of the luminescence excitation spectra. This change in the PLE spectra has been reported for close stacking of perylenes.[75; 76; 77] We extend this formalism to perylene stacking on nanotubes. The closer stacking indicated by these changes is attributed to the higher flexibility of the perylene core in the molecules. The perylene derivative in the most closely stacking molecules is bound to flexible alkyl and PEG chains on both sides. The other three surfactants have alkyl chains on one side and the bulky dendron on the other side, precluding the possibility of stacking as closely.

These results pertaining to the energy transfer characteristics and the excitation channels of the five energy transfer complexes were published as the third of the papers comprising this thesis, Ernst *et al.*, Appl. Phys. Lett. **102**, 233105 (2013).

The close stacking as indicated by the analysis of the quenching behavior of the chromophore is experimentally investigated in high resolution TEM. Figure 3.5 is a micrograph of nanotubes solubilized with a perylene based surfactant. The nanotubes are clearly partially covered in a nanocrystalline material, presumably the surfactant. To

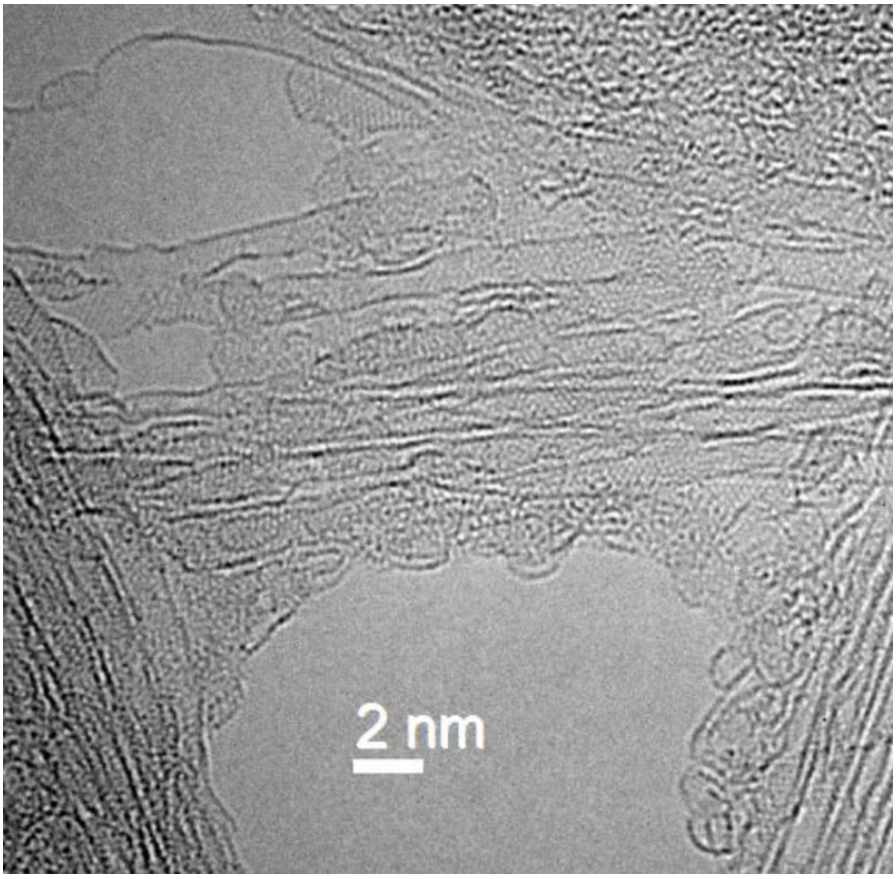

Figure 3.5. High resolution TEM micrograph of carbon nanotubes solubilized with a perylene surfactant. The nanotube is seen to be partially covered by a nanocrystalline material, in all likelihood the surfactant. EELS will be done to confirm.

confirm, EELS measurements are underway. This work is done in collaboration with Raul Arenal in Zaragoza, manuscript in preparation.

Papers four and five, Ernst *et al.*, Phys. Status Solidi (b) **249**, 2465-2468 (2012) and Ernst *et al.*, Phys. Status Solidi (RRL), accepted (2013), concern themselves with the chiral selectivity of the perylene based surfactants. Carbon nanotube solubilization with perylene derived surfactants results in a luminescence intensity distribution across the chiralities that differs markedly from standard bile salt surfactants such as SC. Figure 3.6 shows the intensity differences comparing a HiPco sample solubilized with a perylene based surfactant to the same sample solubilized with SC.

For several chiralities belonging to the same $2n + m = const$ laola family 23 the luminescence is enhanced by several hundred percent. This luminescence intensity increase can have two possible causes: (i) enhanced solubilization through the perylene based sur-

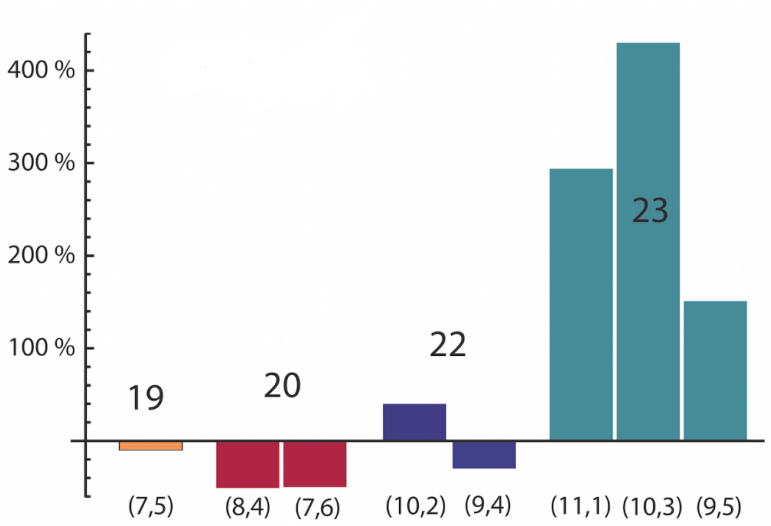

Figure 3.6. Differences in the photoluminescence intensity of different chiralities between HiPco nanotubes solubilized with SC and the same tubes solubilized with a perylene surfactant. Large numbers indicate the $2n + m = const$ laola family.

factant, and (ii) more efficient debundling for certain chiralities. It has been reported that some chiralities have a greater tendency to bundle, resulting in their underrepresentation in luminescence measurements since bundles do not exhibit luminescence.[41]

Resonant Raman measurements are less sensitive to bundling state. By comparing resonant Raman profiles for several tubes between a perylene surfactant solubilized sample and a bile salt reference, we ascertain that the actual abundance of chiralities differs between these samples. Perylene based surfactants preferentially solubilize certain chiralities. However, the differences found in the Raman activity do not account for the entire increase in luminescence intensity.

To determine whether enhanced debundling is also a factor, we resort to the micelle swelling technique, see Sec. 2.3. Nanotubes suspended in bile salt micelles are stirred with DCM. The solvent enters the micelles because their inside is also unpolar, and gradually evaporates. The presence of the organic solvent causes a structural reorganization of the micelles. Generally, luminescence intensity for all chiralities increases, but the degree of enhancement varies. Swelling the micelle with a solvent containing organic chromophores further changes the luminescence intensities. Some chiralities are almost universally enhanced, indicating that the additional chromophore aids the individualization process. We conclude that the perylene unit in the functional surfactants interacts with nanotubes such that it both preferentially solubilizes particular chiralities, and debundles certain tubes more efficiently than bile salt surfactants.

4 | Outlook

In one way, this thesis puts a definite end point to my PhD project: All originally envisaged objectives have been met. That having been said, modification of the nanotube optoelectronic properties in general and creation of energy transfer complexes in particular are very much still an ongoing focus of research for us. For this, my thesis lies the groundwork. In this chapter I will give a brief overview over related research work that is underway.

One advantage of the surfactant-based creation of energy transfer complexes lies in the fact that the working medium is water. Both the functionalization with polymers and the endohedral nanotube filling, approaches (B) and (C) in Fig. 3.1, only work in organic media. The functional surfactant we devised is charge neutral and independent of pH, which, together with the biocompatibility provided by the polyglycerol dendrons, makes our surfactant an ideal candidate for nanotube labeling in biomedical applications. The surfactant does not increase the size of the suspended nanotube compared to traditional biocompatible surfactants such as polysorbates or poloxamers. The additional excitation band provided by the chromophoric unit allows luminescence excitation of all nanotubes at the same wavelength, see Fig. 4.1. This effect is commonly achieved by attaching a traditional fluorophore at the expense of increased size.[78] We tried to use the micelle swelling method to replicate similar systems; however, traditional biocompatible surfactants do not lend themselves to micelle swelling and no biocompatible energy transfer complexes could be produced with these traditional surfactants. A cell viability study is currently underway to test the biocompatibility of perylene surfactant suspended nanotubes, and results look promising.

One of the characteristics of nanotubes much valued in biomedical applications is the fact that their luminescence emission lies in the near infrared, a window of relative optical tissue transparency. Their excitation wavelengths at the respective E_{22} transition energies, however, do not fall into the same window. To counteract this shortcoming, we are functionalizing nanotubes with a two photon absorber entailing a perylene unit

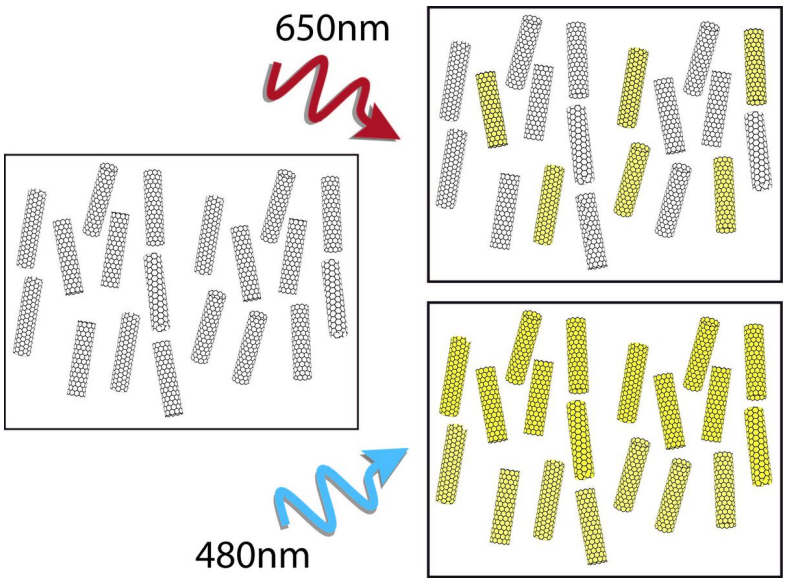

Figure 4.1. Chromophoric surfactants are ideal candidates for labeling carbon nanotubes in vivo: Luminescence excitation at a single wavelength results in a signal from all nanotubes, as opposed to only the chiralities in resonance.

for stacking and energy transfer.[79] Our hope is that this will open an additional two photon absorption band in the NIR. Two photon absorbers are often used in fluorescence imaging because they allow more precise spatial localization and deliver reliable imaging in tissue depths of several 100 μm.[80]

Transient absorption experiments that we have already undertaken in conjunction with Christophe Voisin's group in Paris show that the energy transfer is faster than the experimental response function, i. e., 100 fs. Interestingly, the transfer into the tube becomes less efficient as a function of rising excitation intensity, despite the fact that both chromophore and nanotube on their own behave linearly in this intensity regime. Intriguingly, this behavior is not unique to perylene, but is also found in nanotube energy transfer complexes with other chromophores. The exact dependence of the transfer efficiency on the photon fluence and the causative physical mechanism are currently under investigation.

Very recently, Biswas *et al.* demonstrated the viability of phototransitors based on spectrally sensitized nanotubes in a proof of principle paper.[81] The sensitization itself is done with CdSe-ZnS quantum dots, which were washed over the contacted nanotube. Functionalization with chromophores in the solution phase may lead to an advantage in terms of maximum coverage and temporal stability, as the π-π stacking results in a tight binding between the energy transfer subunits. Using the micelle swelling approach,

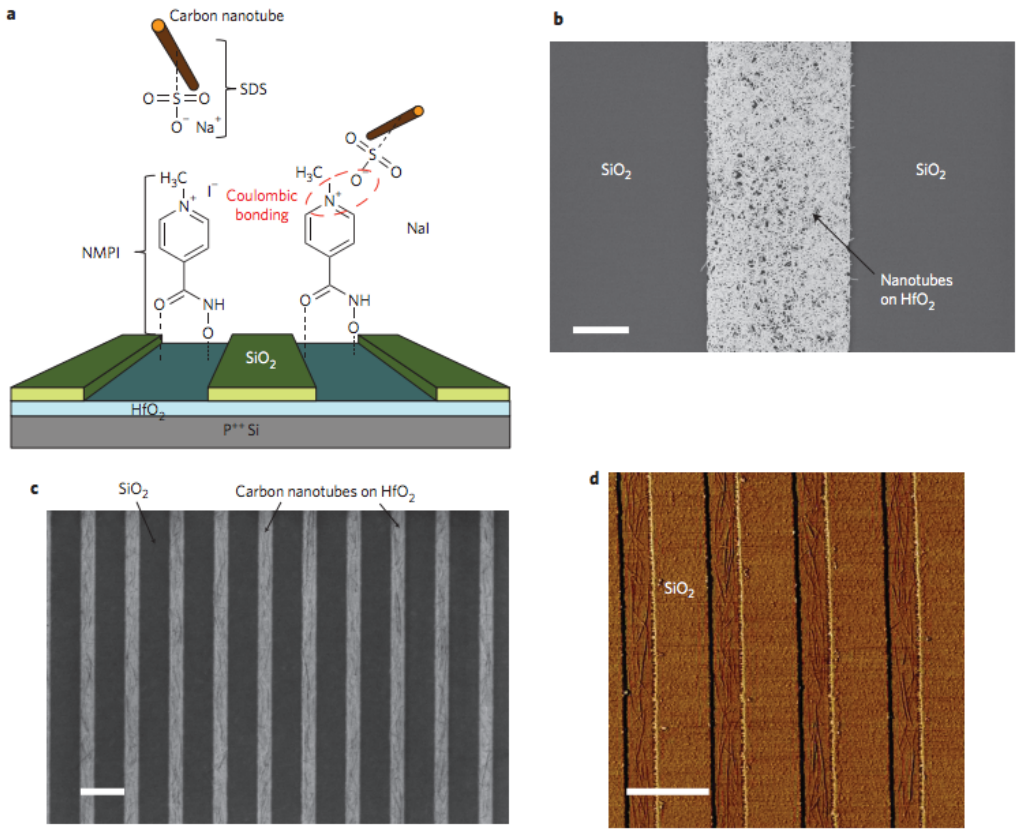

Figure 4.2. Nanotubes suspended in SDS are deposited selectively onto functionalized parts of the substrate via an interaction between the substrate and the SDS. a) Diagrammatic depiction, b) SEM image showing the high coverage afforded by this approach. Scale bar 2 μm. c) SEM and d) AFM images of nanotubes in trenches with widths of 200 nm. Scale bars 500nm. From Ref. [82].

the optical transistor can also be combined with recent groundbreaking advances in the scalability of nanotube assembly into devices. The group around Wilfried Haensch at the IBM Watson Research Center showed that by using selective chemistry on the substrate, SDS solubilized nanotubes can be placed highly efficiently into narrow trenches, see Fig. 4.2 a.[82] Using this method, 10 000 devices are placed on a single chip. Using the micelle swelling technique, the SDS solubilized nanotubes can be functionalized with a chromophore before deposition, making this a promising approach for phototransistors.

Another question we are currently investigating is whether it is possible to transition from an energy transfer system to a charge transfer system in nanotube-chromophore complexes. When an electrochemical potential is applied to such a system it is not mandatory that both Fermi levels shift at the same rate, thus opening the possibility of

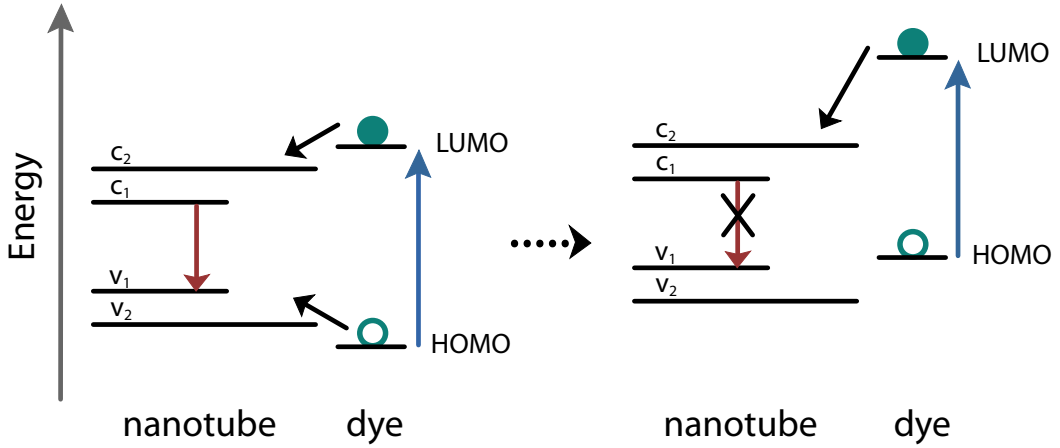

Figure 4.3. Left: Type I heterojunction. Both excited carriers are transferred into the tube. This is the band lineup of all systems investigated in this thesis. When an electrochemical potential is applied, the shift experienced by the subsystems may be disparate, opening the possibility of ending up in a type II heterojunction situation (right). Here, only one of the charge carriers is energetically allowed to transit into the tube. Note that Förster resonance energy transfer is allowed for both type I and type II heterojunctions as it based on a transfer of energy, not a transfer of charge carriers.

transitioning from a type I heterojunction to a type II heterojunction as illustrated in Fig. 4.3. Because the absolute band gap of either system does not change, Förster resonance energy transfer is still allowed in the type II junction. Which mechanism dominates depends on the time scales involved. Unlike double charge transfers as mandated in the Dexter transfer, transfer of single charges may take place on a comparable timescale with the dipole-dipole interaction based Förster resonance.

The last project to come out of this PhD thesis is based on the functionalization with polymers. Certain polymers are known to wrap around nanotubes in a helical fashion, for instance PFO-P, see Fig. 4.4. Note that PFO-P only has sidechains on one side of its backbone. Consequently, functional units can be attached to the other side of the backbone, effectively turning the polymer into a scaffold. PFO-P is a block polymer, which can be functionalized segmentally through a block copolymer approach. This gives us an immensely powerful tool for segmentally modifying the nanotube optical properties, in effect translating well known concepts from the growth of nanowires into their soft-matter equivalent: Nanotubes. A schematic of this approach is shown in Fig. 4.5. Systems we envisage to implement with this approach are manifold. We will give three examples here.

First, serial p-n junctions. Alternating electron and hole donors along the tube yields

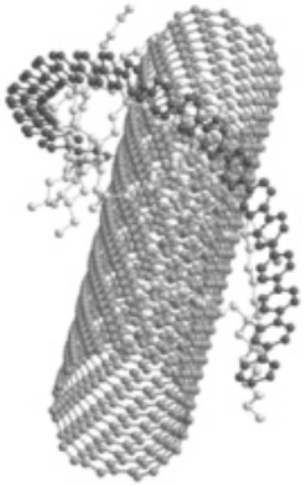

Figure 4.4. Some polymers are known to helically wrap around nanotubes, such as PFO-P, here as calculated in a molecular dynamics simulation. Note that this polymer only has sidechains on one side of its backbone. From Ref. [49].

segmental doping. Electron and hole doped sections will alternate, resulting in a very high density of p-n junctions at the borders between the segments in the nanotube. So, upon radiative excitation of the p- and n-donors, holes and electrons respectively will enter the tube. Nanotubes intrinsically emit in the NIR, so when charge carriers recombine at the segment borders, the nanotube turns into a mesoscopic LED with an emission in the near infrared.

Second, spin-polarized transport. To achieve spin-polarized transport through the nanotube, we will attach single molecule magnets, in this case Mn_{12}, to the PFO-P scaffold. Mn_{12} molecular magnets have a total spin $S = 10$,[83] which is enough to lift the spin degeneracy of the electronic ground state in nanotubes, see Sec. 2.1.2, provided the distance between nanotube and single molecule magnet is 1 nm or smaller, resulting in magnetic fields of several 100 mT.[84] These distances are achievable in the PFO-P polymer functionalization. By aligning the single molecule magnets once in an external magnetic field, the electronic ground state for one spin state is lowered, while the electronic ground state for the other spin state is elevated. At low temperatures, this induces a blockade for carriers of one spin type, see Fig. 4.6.

The third functionalization results in serial quantum dots. Again Mn_{12} molecular magnets are used, however, now the functionalized segments of the PFO-P are alternated

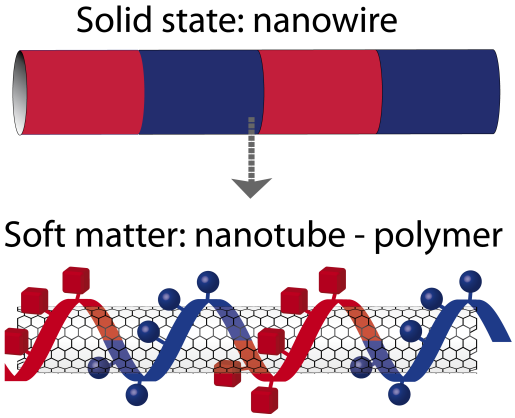

Figure 4.5. Nanowires can be grown such that their optoelectronic properties change along the length of the wire. So far, this has been impossible for nanotubes. We will use a helically wrapping polymer, PFO-P, as a scaffold for functional units. PFO-P can be functionalized segmentally with different functional units, effectively dividing the nanotube into sections with disparate optoelectronic properties.

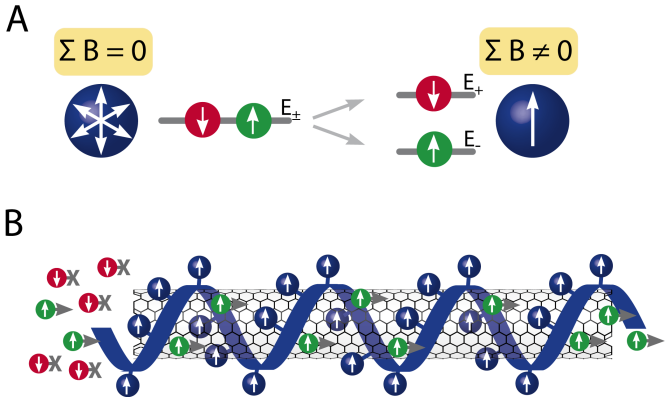

Figure 4.6. A carbon nanotube is decorated with Mn_{12} molecular magnets via the PFO-P scaffold along its length. The resulting magnetic field lifts the degeneracy of the electronic ground state with respect to spin. The electronic ground state for spin up electrons is lowered, while the ground state for spin down electrons is elevated. At low temperatures, this results in a spin blockade for spin down electrons.

with non-functionalized segments, creating a series of quantum wells for carriers of one spin type. By making the functionalized segments short enough, quantum dots are created. This is of great interest, for instance for quantum computing applications, since carbon-based systems have exceptionally long spin decoherence times. Up to now, quantum dots in carbon nanotubes are mostly prepared by placing electrodes around the nanotube after deposition. Solution-phase processing and subsequent deposition make this costly step superfluous.

In conclusion, I hope that this brief overview of research projects currently underway has demonstrated that the creation of nanotube-chromophore energy transfer complexes for us was only the first chapter in the tailoring of nanotube optoelectronics. Understanding the molecular interactions between functional subunits can be capitalized on for designing intricate, yet scalable, self-assembly processes in nanotechnology. The future is full of promise for the solution-phase creation of complex quantum systems.

Appendix

A | Methods

A.1. Sample preparation

A.1.1. Nanotube suspension with perylene surfactants

The success of suspending nanotubes with perylene surfactants depends critically on the solubilization parameters. When too little surfactant is used, nanotubes are not debundled sufficiently, resulting in the quenching of the luminescence. On the other hand, when too much surfactant is used, the hot luminescence of the perylene in the infrared masks large parts of the underlying spectrum. An example of moderate masking by excess perylene surfactant is shown in Fig. A.1. Vexingly, it is not only the ratio of nanotube to surfactant concentration that has to be determined, but the absolute concentration of both. The amount of free surfactant interfering with optical measurements depends on the dynamic equilibrium between adsorbed surfactant and free surfactant. By adding more solvent to a perfect solution it can be made unusable for spectroscopic analysis. Consequently, devising a good sample preparation protocol is an optimization process in two parameters.

Because of the problem of masking we worked at low perylene surfactant concentrations between $1 \cdot 10^{-5}$ M and $8 \cdot 10^{-5}$ M. The best results were obtained for concentrations of $6 \cdot 10^{-5}$ M. Fig. A.2 (a) shows the dependence of the perylene fluorescence signal in the visible after an excitation at the surfactant's absorption maximum at 495 nm as a function of the nanotube preparation concentration ranging from 0.01 g/l to 0.15 g/l. By varying the nanotube concentration by one order of magnitude, the fluorescence is quenched by a factor of 10^4. Fig. A.2 (b) shows the same samples after the same excitation in the perylene's absorption band in the infrared emission range. This is the emission from the nanotubes subsequent to the energy transfer. The nanotube signal rises as a function of preparation concentration up to 0.09 g/l, and falls hereafter. The nanotube luminescence falls although the nanotube preparation concentration rises because there is too little

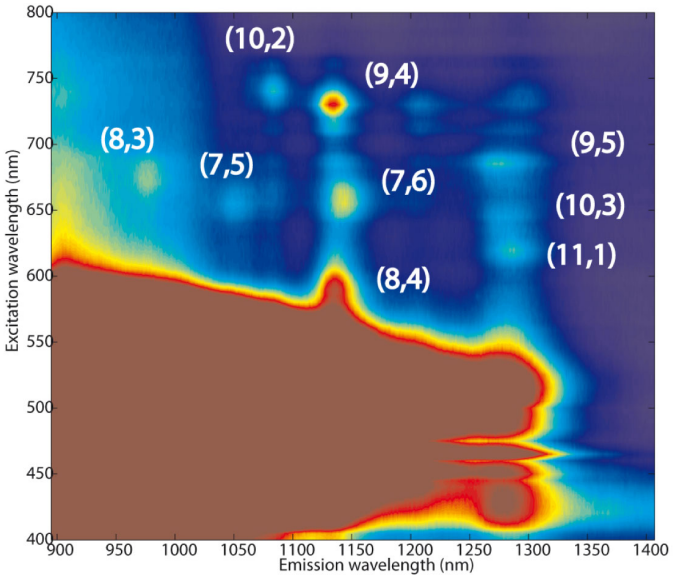

Figure A.1. HiPco nanotubes solubilized with a perylene based surfactant. Excess of surfactant results in the masking of large spectral regions.

surfactant to debundle the tubes, resulting in luminescence quenching.

Fig. A.2 demonstrates that finding the right concentrations for efficient solubilization of nanotubes with the perylene surfactant is difficult. However, note that the fluorescence of the perylene is quenched for a NT preparation concentration of 0.11 g/l, while the corresponding emission from the nanotube is strong. This indicates that once the right concentrations have been worked out, the perylene surfactant suspends individualized nanotubes with almost no free surfactant in the solution. This is also apparent from the photoluminescence maps shown in this manuscript, see, for instance, Fig. 2.12. The resulting samples are stable over many months and the sample preparation process is very reliable: Once the correct parameters are determined, good samples are produced faithfully.

The preparation protocol for **C16**: 0.11 g/l HiPco SWNTs (Unidym, batch SP0295) are solubilized with $6 \cdot 10^{-5}$ M of surfactant. A 5 ml sample is tip sonicated in a Bandelin Sonopuls 2070 with a 3 mm titanium tip at 30 % intensity, 300 ms per second, for 90 min at room temperature. Subsequently the sample is centrifuged at 31 500 g and 18° C in a Hettich MIKRO 220R tabletop microliter centrifuge. The supernatant is carefully pipetted off, the rest is discarded.

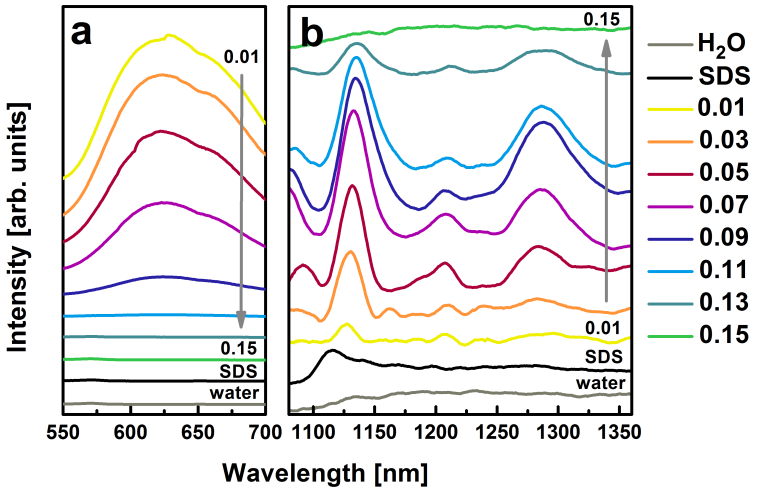

Figure A.2. Photoluminescence intensity of perylene surfactant (a) and carbon nanotubes after energy transfer (b) as a function of nanotube preparation concentration. The excitation wavelength for both emission ranges is 495 nm, in the absorption band of the perylene surfactant. Note that the SDS solubilized sample shows no signal in either emission range as nanotubes have no intrinsic resonance at 495 nm.

A.1.2. Micelle swelling

0.1 g/l HiPco SWNTs (Unidym, batch SP0295) are solubilized with 2 wt% SC in deionized water. A 10 ml sample is tip sonicated in a Bandelin Sonopuls 2070 with a 3 mm titanium tip at 30 % intensity, 300 ms per second, for 60 min at room temperature. Subsequently the sample is centrifuged at 31 500 g and 23° C in a Hettich MIKRO 220R tabletop microliter centrifuge. The supernatant is carefully pipetted off, the rest is discarded. Photoluminescence and absorption of the sample are measured to ensure the nanotubes are well dispersed.

For the micelle swelling we found dichloromethane (DCM) is the best solvent to use. It is immiscible with water, volatile and has a density of 1.33 g/cm^3. Chromophoric DCM solutions are prepared at a concentration of 1 g/l. To 2 ml of nanotube-SC solution 0.2 ml of chromophoric DCM solution is added. The sample is tip sonicated at 10 % intensity and 500 ms per second for 5 min at room temperature, then stirred at 500 rpm for 24 h without lid. After this period all DCM has evaporated. The sample is centrifuged again, the supernatant pipetted off, the rest discarded. This protocoll was found to work for anthracene, pyrene, m-terphenyl, o-terphenyl, p-terphenyl, nile red, α-quaterthiophene (α4T), and dihexylsexithiophene (DH6T), resulting in chromophore-nanotube complexes

suspended in SC micelles. The solutions are temporally stable.

The protocol does not work for perylene or perylene derivative dyes. Extensive experimentation with different solvents, surfactants, sonication and stirring parameters did not result in satisfactory samples. This is attributed to the fact that perylenes form stacks in solution which are bulky and not amenable to micelle swelling.

A.2. Spectroscopic methods

All photoluminescence measurements were performed in a Horiba Jobin Yvon NanoLog, see Fig. A.3. The excitation source is a 450 W Xenon short arc lamp, which extends from the UV to the near IR. A single excitation line is selected with a monochromator with two mechanically coupled gratings (1200 grooves/mm, blazed at 500nm). Sample compartments for both liquid and solid samples are in use. Light can either be collected in front face or right angle configuration, the latter only works for liquid samples of low optical density. Samples with high optical densities do not yield a signal at all owing to absorption. Care has to be taken with right angle data from samples with intermediate optical densities. These spectra may suffer from reabsorption effects. Corresponding beam paths are indicated in Fig. A.3. Behind the sample compartment, the NanoLog features a triple-grating turret with three gratings (1200 grooves/mm, blazed at 500 nm; 600 grooves/mm, blazed at 1000 nm; 150 grooves/mm, blazed at 1200 nm) and two detectors, a photodiode for the visible (240 nm-1000 nm) and an InGaAs multi-channel detector for the near IR (900 nm-1580 nm). Filters were used where necessary.

A blank was subtracted from all data, accounting for detector effects, and a lamp correction was performed. Where luminescence intensities were extracted, we fitted every peak with a Lorentzian and subtracted linear and constant background. As specified in the papers, either peak volume or peak height were used as a proxy for peak intensity. All analysis was performed in Mathematica and MATLAB.

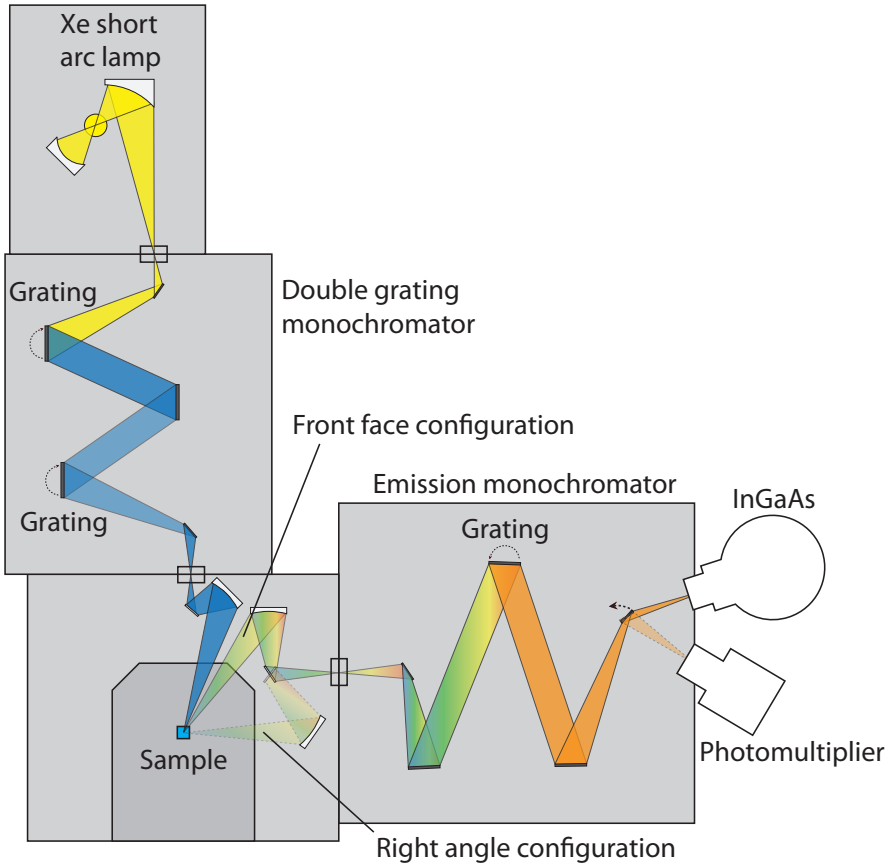

Figure A.3. Schematic diagram of the NanoLog photoluminescence spectrometer, see text for details. Adapted from Ref [85].

Acknowledgements

Throughout the past three years at the Freie Universität Berlin I was lucky enough to receive support and assistance from many people. I would like to thank ...

... first and foremost my supervisor, Stephanie Reich, for providing me with a well thought out thesis project and unrelenting support throughout the past three years. She gave me the freedom to explore the avenues I wanted to explore, but never failed to point out the experiments she thought relevant. During my time here I have learned much more from her than I could possibly list, ranging from outright physics questions to figuring out which problems to look at, from starting and maintaining collaborations to writing papers and proposals.

... Antonio Setaro. Antonio was of great help to me throughout my PhD (mathematica-, physics-, and otherwise!), as well as fantastic to share an office with.

... Timm Heek and Rainer Haag from the department of chemistry of the Freie Universität, with whom I enjoyed a very fruitful collaboration: Rainer and Timm were responsible for the synthesis of all functional surfactants covered in this thesis.

... Nacho Pascual for being my second supervisor, making me feel I could come to him with problems (which luckily never arose), and coming back to Berlin for my defense.

... Ludger Wöste, Jenny Schlüpmann, and Mathieu Lalanne for being in my PhD committee.

... Gudrun May-Nasseri for taking care of travel approvals, orders, and forms of all sorts and sizes almost always before they drove me crazy. Thanks, also, for being the good soul of the group and overseeing the coffee stocks!

... the entire AG Reich. They were indispensable for support, conversation and (of

course only very occasionally) entertainment. Thanks, Sebastian Heeg, Mareen Gläske, Benjamin Hatting, Patryk Kusch, Pascal Blümmel, Philip Klar, Stefanie Kreft, and the rest of the gang.

It is with tremendous gratitude that I leave the physics department of the Freie Universität Berlin.

Last, but not least, I would like to thank my family.

Curriculum Vitae

For reasons of data protection, the curriculum vitae is not included in the online version.

Publications

1. Energy Transfer in Nanotube-Perylene Complexes
   F. Ernst, T. Heek, A. Setaro, R. Haag, and S. Reich
   Adv. Funct. Mater. **22**, 3921-3926 (2012).
   (Shared first authorship with T. Heek)

   T. Heek synthesized and characterized the functional surfactant under the supervision of R. Haag. I prepared the samples, performed the experiments and analyzed the data. A. Setaro and S. Reich contributed to the theoretical interpretation. I wrote the manuscript and all authors commented on it. The project was envisaged by S. Reich, R. Haag, and A. Setaro.

2. Chirally enhanced solubilization through perylene-based surfactant
   F. Ernst, T. Heek, R. Haag, S. Reich, and A. Setaro
   Phys. Status Solidi (b) **249**, 2465-2468 (2012).

   T. Heek synthesized the functional surfactant under the supervision of R. Haag. I prepared the samples, performed the experiments and analyzed the data. A. Setaro and S. Reich contributed to the theoretical interpretation. I wrote the manuscript and all authors commented on it. The project was envisaged by A. Setaro, S. Reich, and me.

3. Functional Surfactants for Carbon Nanotubes: Effect of Design
   F. Ernst, T. Heek, A. Setaro, R. Haag, and S. Reich
   J. Phys. Chem. C **117**, 1157-1162 (2013).

   T. Heek synthesized and characterized the functional surfactants under the supervision of R. Haag. I prepared the samples, performed the experiments and analyzed the data. A. Setaro and S. Reich contributed to the theoretical interpretation. I wrote the manuscript and all authors commented on it. The project was envisaged by S. Reich, R. Haag, and A. Setaro.

4. Excitation characteristics of different energy transfer in nanotube-perylene complexes
   F. Ernst, T. Heek, A. Setaro, R. Haag, and S. Reich
   Appl. Phys. Lett. **102**, 233105 (2013).

   T. Heek synthesized and characterized the functional surfactant under the supervision of R. Haag. I prepared the samples, performed the experiments and analyzed the data. A. Setaro and S. Reich contributed to the theoretical interpretation. I wrote the manuscript and all authors commented on it. The project was envisaged by S. Reich and me.

5. Selective interaction between nanotubes and perylene based surfactant
   F. Ernst, S. Heeg, T. Heek, A. Setaro, R. Haag, and S. Reich
   Phys. Status Solidi (RRL), doi 10.1002/pssr.201307221 (2013).

   T. Heek synthesized and characterized the functional surfactant under the supervision of R. Haag. I prepared the samples. S. Heeg performed the resonant Raman measurements. I performed the photoluminescence measurements and analyzed the data. S. Reich contributed to the theoretical interpretation. I wrote the manuscript and all authors commented on it. The project was envisaged by S. Reich and me.

Bibliography

[1] Vikram V Deshpande, Marc Bockrath, Leonid I Glazman, and Amir Yacoby. Electron liquids and solids in one dimension. *Nature*, 464(7286):209–16, March 2010.

[2] I. L. Aleiner, B. L. Altshuler, and G. V. Shlyapnikov. A finite-temperature phase transition for disordered weakly interacting bosons in one dimension. *Nature Physics*, 6(11):900–904, September 2010.

[3] Jean-Christophe Charlier and Stephan Roche. Electronic and transport properties of nanotubes. *Reviews of Modern Physics*, 79(2):677–732, May 2007.

[4] Eric Pop, David Mann, Qian Wang, Kenneth Goodson, and Hongjie Dai. Thermal conductance of an individual single-wall carbon nanotube above room temperature. *Nano letters*, 6(1):96–100, January 2006.

[5] M. Yu. Strength and Breaking Mechanism of Multiwalled Carbon Nanotubes Under Tensile Load. *Science*, 287(5453):637–640, January 2000.

[6] Rüdiger Klingeler and Robert B. Sim. *Carbon Nanotubes for Biomedical Applications*. Springer, 2011.

[7] Friedrich Schoppler, Christoph Mann, Tilman C. Hain, Felix M. Neubauer, Giulia Privitera, Francesco Bonaccorso, Daping Chu, Andrea C. Ferrari, and Tobias Hertel. Molar Extinction Coefficient of Single-Wall Carbon Nanotubes. *The Journal of Physical Chemistry C*, 115(30):14682–14686, August 2011.

[8] Yang Zhao, Ai-Min Ren, Ji-Kang Feng, and Chia-Chung Sun. Theoretical study of one-photon and two-photon absorption properties of perylene tetracarboxylic derivatives. *The Journal of chemical physics*, 129(1):014301, July 2008.

[9] Friederike Ernst, Timm Heek, Antonio Setaro, Rainer Haag, and Stephanie Reich. Energy Transfer in Nanotube-Perylene Complexes. *Advanced Functional Materials*, 22:3921 – 3926, May 2012.

[10] Friederike Ernst, Timm Heek, Antonio Setaro, Rainer Haag, and Stephanie Reich. Excitation characteristics of different energy transfer in nanotube-perylene complexes. *Applied Physics Letters*, 102(23):233105, 2013.

[11] R. Martel, V. Derycke, C. Lavoie, J. Appenzeller, K. Chan, J. Tersoff, and Ph. Avouris. Ambipolar Electrical Transport in Semiconducting Single-Wall Carbon Nanotubes. *Physical Review Letters*, 87(25):256805, December 2001.

[12] T. Dürkop, S. a. Getty, Enrique Cobas, and M. S. Fuhrer. Extraordinary Mobility in Semiconducting Carbon Nanotubes. *Nano Letters*, 4(1):35–39, January 2004.

[13] Satria Zulkarnaen Bisri, Jia Gao, Vladimir Derenskyi, Widianta Gomulya, Igor Iezhokin, Pavlo Gordiichuk, Andreas Herrmann, and Maria Antonietta Loi. High performance ambipolar field-effect transistor of random network carbon nanotubes. *Advanced materials (Deerfield Beach, Fla.)*, 24(46):6147–52, December 2012.

[14] Yi Zhang, Yuhong Bai, and Bing Yan. Functionalized carbon nanotubes for potential medicinal applications. *Drug discovery today*, 15(11-12):428–35, June 2010.

[15] Monika Wyszogrodzka and Rainer Haag. Study of single protein adsorption onto monoamino oligoglycerol derivatives: a structure-activity relationship. *Langmuir : the ACS journal of surfaces and colloids*, 25(10):5703–12, May 2009.

[16] Sumio Iijima. Helical microtubules of graphitic carbon. *Nature*, 354(6348):56–58, November 1991.

[17] Sumio Iijima and Toshinari Ichihashi. Single-shell carbon nanotubes of 1-nm diameter. *Nature*, 363(6430):603–605, June 1993.

[18] D. S. Bethune, C. H. Klang, M. S. de Vries, G. Gorman, R. Savoy, J. Vazquez, and R. Beyers. Cobalt-catalysed growth of carbon nanotubes with single-atomic-layer walls. *Nature*, 363(6430):605–607, June 1993.

[19] Noriaki Hamada, Shin-ichi Sawada, and Atsushi Oshiyama. New one-dimensional conductors: Graphitic microtubules. *Physical Review Letters*, 68(10):1579–1581, March 1992.

[20] R. Saito, M. Fujita, G. Dresselhaus, and M. S Dresselhaus. Electronic structure of chiral graphene tubules. *Applied Physics Letters*, 60(18):2204, 1992.

[21] S. Reich, C. Thomsen, and J. Maultzsch. *Carbon Nanotubes*. WILEY-VCH, 2004.

[22] Tsuneya Ando. The electronic properties of graphene and carbon nanotubes. *NPG Asia Materials*, 1(1):17–21, October 2009.

[23] J. Mintmire and C. White. Universal Density of States for Carbon Nanotubes. *Physical Review Letters*, 81(12):2506–2509, September 1998.

[24] Hiroshi Ajiki and Tsuneya Ando. Aharonov-Bohm effect in carbon nanotubes. *Physica B: Condensed Matter*, 201:349–352, July 1994.

[25] Sergei M Bachilo, Michael S Strano, Carter Kittrell, Robert H Hauge, Richard E Smalley, and R Bruce Weisman. Structure-assigned optical spectra of single-walled carbon nanotubes. *Science*, 298(5602):2361–6, December 2002.

[26] Catalin Spataru, Sohrab Ismail-Beigi, Lorin Benedict, and Steven Louie. Excitonic Effects and Optical Spectra of Single-Walled Carbon Nanotubes. *Physical Review Letters*, 92(7):077402, February 2004.

[27] Eric Chang, Giovanni Bussi, Alice Ruini, and Elisa Molinari. Excitons in Carbon Nanotubes: An Ab Initio Symmetry-Based Approach. *Physical Review Letters*, 92(19):196401, May 2004.

[28] Feng Wang, Gordana Dukovic, Louis E Brus, and Tony F Heinz. The optical resonances in carbon nanotubes arise from excitons. *Science (New York, N.Y.)*, 308(5723):838–41, May 2005.

[29] J. Maultzsch, R. Pomraenke, S. Reich, E. Chang, D. Prezzi, a. Ruini, E. Molinari, M. Strano, C. Thomsen, and C. Lienau. Exciton binding energies in carbon nanotubes from two-photon photoluminescence. *Physical Review B*, 72(24):1–4, December 2005.

[30] Catalin Spataru, Sohrab Ismail-Beigi, Rodrigo Capaz, and Steven Louie. Quasiparticle and Excitonic Effects in the Optical Response of Nanotubes and Nanoribbons. In Ado Jorio, Mildred Dresselhaus, and Gene Dresselhaus, editors, *Carbon Nanotubes, Topics Appl. Physics 111*, pages 195–227. 2008.

[31] Vasili Perebeinos, J. Tersoff, and Phaedon Avouris. Scaling of Excitons in Carbon Nanotubes. *Physical Review Letters*, 92(25):257402, June 2004.

[32] Michael J O'Connell, Sergei M Bachilo, Chad B Huffman, Valerie C Moore, Michael S Strano, Erik H Haroz, Kristy L Rialon, Peter J Boul, William H Noon, Carter Kittrell, Jianpeng Ma, Robert H Hauge, R Bruce Weisman, and Richard E Smalley. Band gap fluorescence from individual single-walled carbon nanotubes. *Science (New York, N.Y.)*, 297(5581):593–6, July 2002.

[33] C. Manzoni, A. Gambetta, E. Menna, M. Meneghetti, G. Lanzani, and G. Cerullo. Intersubband Exciton Relaxation Dynamics in Single-Walled Carbon Nanotubes. *Physical Review Letters*, 94(20):207401, May 2005.

[34] Vasili Perebeinos, J Tersoff, and Phaedon Avouris. Radiative lifetime of excitons in carbon nanotubes. *Nano letters*, 5(12):2495–9, December 2005.

[35] Catalin Spataru, Sohrab Ismail-Beigi, Rodrigo Capaz, and Steven Louie. Theory and AbInitio Calculation of Radiative Lifetime of Excitons in Semiconducting Carbon Nanotubes. *Physical Review Letters*, 95(24):247402, December 2005.

[36] Feng Wang, Gordana Dukovic, Louis Brus, and Tony Heinz. Time-Resolved Fluorescence of Carbon Nanotubes and Its Implication for Radiative Lifetimes. *Physical Review Letters*, 92(17):177401, April 2004.

[37] C.-X. Sheng, Z. Vardeny, A. Dalton, and R. Baughman. Exciton dynamics in single-walled nanotubes: Transient photoinduced dichroism and polarized emission. *Physical Review B*, 71(12):125427, March 2005.

[38] Jacques Lefebvre, David G Austing, Jeffery Bond, and Paul Finnie. Photoluminescence imaging of suspended single-walled carbon nanotubes. *Nano letters*, 6(8):1603–8, August 2006.

[39] R. Saito, G. Dresselhaus, and M. Dresselhaus. Trigonal warping effect of carbon nanotubes. *Physical Review B*, 61(4):2981–2990, January 2000.

[40] Ge. G. Samsonidze, R. Saito, N. Kobayashi, A. Gruneis, J. Jiang, A. Jorio, S. G. Chou, G. Dresselhaus, and M. S. Dresselhaus. Family behavior of the optical transition energies in single-wall carbon nanotubes of smaller diameters. *Applied Physics Letters*, 85(23):5703, 2004.

[41] Carolin Blum, Ninette Stürzl, Frank Hennrich, Sergei Lebedkin, Sebastian Heeg, Heiko Dumlich, Stephanie Reich, and Manfred M Kappes. Selective bundling of zigzag single-walled carbon nanotubes. *ACS nano*, 5(4):2847–54, April 2011.

[42] Mark C Hersam. Progress towards monodisperse single-walled carbon nanotubes. *Nature nanotechnology*, 3(7):387–94, July 2008.

[43] Michael S Strano, Christopher a Dyke, Monica L Usrey, Paul W Barone, Mathew J Allen, Hongwei Shan, Carter Kittrell, Robert H Hauge, James M Tour, and Richard E Smalley. Electronic structure control of single-walled carbon nanotube functionalization. *Science (New York, N.Y.)*, 301(5639):1519–22, September 2003.

[44] Takeshi Tanaka, Hehua Jin, Yasumitsu Miyata, Shunjiro Fujii, Hiroshi Suga, Yasuhisa Naitoh, Takeo Minari, Tetsuhiko Miyadera, Kazuhito Tsukagoshi, and Hiromichi Kataura. Simple and Scalable Gel-Based Semiconducting Carbon Nanotubes 2009. *Nano Letters*, 2:2–5, 2009.

[45] Takeshi Tanaka, Yasuko Urabe, Daisuke Nishide, and Hiromichi Kataura. Continuous Separation of Metallic and Semiconducting Carbon Nanotubes Using Agarose Gel. *Applied Physics Express*, 2(12):125002, November 2009.

[46] Huaping Liu, Daisuke Nishide, Takeshi Tanaka, and Hiromichi Kataura. Large-scale single-chirality separation of single-wall carbon nanotubes by simple gel chromatography. *Nature communications*, 2(May):309, January 2011.

[47] Saunab Ghosh, Sergei M Bachilo, and R Bruce Weisman. Advanced sorting of single-walled carbon nanotubes by nonlinear density-gradient ultracentrifugation. *Nature nanotechnology*, 5(6):443–50, June 2010.

[48] Adrian Nish, Jeong-Yuan Hwang, James Doig, and Robin J Nicholas. Highly selective dispersion of single-walled carbon nanotubes using aromatic polymers. *Nature nanotechnology*, 2(10):640–6, October 2007.

[49] Jeong-Yuan Hwang, Adrian Nish, James Doig, Sigrid Douven, Chun-Wei Chen, Li-Chyong Chen, and Robin J Nicholas. Polymer structure and solvent effects on the selective dispersion of single-walled carbon nanotubes. *Journal of the American Chemical Society*, 130(11):3543–53, March 2008.

[50] Xueying Huang, Robert S Mclean, and Ming Zheng. High-Resolution Length Sorting and Purification of DNA-Wrapped Carbon Nanotubes by Size-Exclusion Chromatography. *Anal. Chem.*, 77(19):6225–6228, 2005.

[51] Xiaomin Tu, Suresh Manohar, Anand Jagota, and Ming Zheng. DNA sequence motifs for structure-specific recognition and separation of carbon nanotubes. *Nature*, 460(7252):250–3, July 2009.

[52] Ming Zheng, Anand Jagota, Michael S Strano, Adelina P Santos, Paul Barone, S Grace Chou, Bruce A Diner, Mildred S Dresselhaus, Robert S McLean, G Bibiana Onoa, Georgii G Samsonidze, Ellen D Semke, Monica Usrey, and Dennis J Walls. Structure-based carbon nanotube sorting by sequence-dependent DNA assembly. *Science (New York, N.Y.)*, 302(5650):1545–8, November 2003.

[53] Antonio Setaro, Chris S. Popeney, Britta Trappmann, Rainer Haag, and Stephanie Reich. Interaction between single-walled carbon nanotubes and alkyl-polyglycerol derivatives. *physica status solidi (b)*, 247(11-12):2758–2761, December 2010.

[54] A. Setaro, C.S. Popeney, B. Trappmann, V. Datsyuk, R. Haag, and S. Reich. Polyglycerol-derived amphiphiles for single walled carbon nanotube suspension. *Chemical Physics Letters*, 493(1-3):147–150, June 2010.

[55] Friederike Ernst, Timm Heek, Rainer Haag, Stephanie Reich, and Antonio Setaro. Chirally enhanced solubilization through perylene-based surfactant. *physica status solidi (b)*, 249(12):2465–2468, December 2012.

[56] Friederike Ernst, Sebastian Heeg, Timm Heek, Antonio Setaro, Rainer Haag, and Stephanie Reich. Selective interaction between nanotubes and perylene based surfactant. *physica status solidi (RRL) - Rapid Research Letters*, 2013.

[57] Bernhard Valeur and Mario Nuno Berberan-Santos. *Molecular Fluorescence*. WILEY-VCH, 2012.

[58] Robert M Clegg. The history of FRET : From conception through the labors of birth. In Chris D. Geddes and Joseph R. Lakowicz, editors, *Reviews in Fluorescence 2006*, pages 1–45. Springer, 2006.

[59] Liangwei Qu, Robert B. Martin, Weijie Huang, Kefu Fu, Daniel Zweifel, Yi Lin, Ya-Ping Sun, Christopher E. Bunker, Barbara a. Harruff, James R. Gord, and Lawrence F. Allard. Interactions of functionalized carbon nanotubes with tethered pyrenes in solution. *The Journal of Chemical Physics*, 117(17):8089, 2002.

[60] W. Feng, A. Fujii, M. Ozaki, and K. Yoshino. Perylene derivative sensitized multi-walled carbon nanotube thin film. *Carbon*, 43(12):2501–2507, October 2005.

[61] Kazuhiro Yanagi, Konstantin Iakoubovskii, Hiroyuki Matsui, Hiroyuki Matsuzaki, Hiroshi Okamoto, Yasumitsu Miyata, Yutaka Maniwa, Said Kazaoui, Nobutsugu Minami, and Hiromichi Kataura. Photosensitive function of encapsulated dye in carbon nanotubes. *Journal of the American Chemical Society*, 129(16):4992–7, April 2007.

[62] Adrian Nish, Jeong-Yuan Hwang, James Doig, and Robin J Nicholas. Direct spectroscopic evidence of energy transfer from photo-excited semiconducting polymers to single-walled carbon nanotubes. *Nanotechnology*, 19(9):095603, March 2008.

[63] Friederike Ernst, Timm Heek, Antonio Setaro, Rainer Haag, and Stephanie Reich. Functional Surfactants for Carbon Nanotubes: Effects of Design. *The Journal of Physical Chemistry C*, 117(2):1157–1162, January 2013.

[64] Randy K Wang, Wei-Chiang Chen, Daisy K Campos, and Kirk J Ziegler. Swelling the micelle core surrounding single-walled carbon nanotubes with water-immiscible organic solvents. *Journal of the American Chemical Society*, 130(48):16330–7, December 2008.

[65] Cyrielle Roquelet, Jean-Sébastien Lauret, Valérie Alain-Rizzo, Christophe Voisin, Romain Fleurier, Morgan Delarue, Damien Garrot, Annick Loiseau, Philippe Roussignol, Jacques A Delaire, and Emmanuelle Deleporte. Pi-stacking functionalization of carbon nanotubes through micelle swelling. *Chemphyschem : a European journal of chemical physics and physical chemistry*, 11(8):1667–72, June 2010.

[66] C. Roquelet, D. Garrot, J. S. Lauret, C. Voisin, V. Alain-Rizzo, Ph. Roussignol, J. a. Delaire, and E. Deleporte. Quantum efficiency of energy transfer in noncovalent carbon nanotube/porphyrin compounds. *Applied Physics Letters*, 97(14):141918, 2010.

[67] Damien Garrot, Benjamin Langlois, Cyrielle Roquelet, Thierry Michel, Philippe Roussignol, Claude Delalande, Emmanuelle Deleporte, Jean-Sébastien Lauret, and Christophe Voisin. Time-Resolved Investigation of Excitation Energy Transfer in Carbon NanotubePorphyrin Compounds. *The Journal of Physical Chemistry C*, 115(47):23283–23292, December 2011.

[68] Cyrielle Roquelet, Fabien Vialla, Carole Diederichs, Philippe Roussignol, Claude Delalande, Emmanuelle Deleporte, Jean-Sébastien Lauret, and Christophe Voisin. Local field effects in the energy transfer between a chromophore and a carbon nanotube: a single-nanocompound investigation. *ACS nano*, 6(10):8796–802, October 2012.

[69] Andreas Hirsch. Functionalization of Single-Walled Carbon Nanotubes. *Angewandte Chemie International Edition*, 41(11):1853, June 2002.

[70] F. Tournus, S. Latil, M. Heggie, and J.-C. Charlier. Π-Stacking Interaction Between Carbon Nanotubes and Organic Molecules. *Physical Review B*, 72(7):075431, August 2005.

[71] Holger Frey and Rainer Haag. Dendritic polyglycerol: a new versatile biocompatible-material. *Journal of biotechnology*, 90(3-4):257–67, May 2002.

[72] Holger Frey and Rainer Haag. Dendritic polyglycerol: a new versatile biocompatible material. *Reviews in Molecular Biotechnology*, 90(3-4):257–267, 2002.

[73] Monika Wyszogrodzka and Rainer Haag. A convergent approach to biocompatible polyglycerol "click" dendrons for the synthesis of modular core-shell architectures and their transport behavior. *Chemistry (Weinheim an der Bergstrasse, Germany)*, 14(30):9202–14, January 2008.

[74] Monika Wyszogrodzka and Rainer Haag. Synthesis and characterization of glycerol dendrons, self-assembled monolayers on gold: a detailed study of their protein resistance. *Biomacromolecules*, 10(5):1043–54, May 2009.

[75] J. Seibt, P. Marquetand, Volker Engel, Z. Chen, V. Dehm, and F. Würthner. On the geometry dependence of molecular dimer spectra with an application to aggregates of perylene bisimide. *Chemical Physics*, 328(1-3):354–362, September 2006.

[76] Reinhold F Fink, Joachim Seibt, Volker Engel, Manuel Renz, Martin Kaupp, Stefan Lochbrunner, Hong-Mei Zhao, Johannes Pfister, Frank Würthner, and Bernd Engels. Exciton trapping in pi-conjugated materials: a quantum-chemistry-based protocol applied to perylene bisimide dye aggregates. *Journal of the American Chemical Society*, 130(39):12858–9, October 2008.

[77] Frank Würthner, Theo E Kaiser, and Chantu R Saha-Möller. J-aggregates: from serendipitous discovery to supramolecular engineering of functional dye materials. *Angewandte Chemie (International ed. in English)*, 50(15):3376–410, April 2011.

[78] Shige H Yoshimura, Shahbaz Khan, Hiroyuki Maruyama, Yoshikazu Nakayama, and Kunio Takeyasu. Fluorescence labeling of carbon nanotubes and visualization of a nanotube-protein hybrid under fluorescence microscope. *Biomacromolecules*, 12(4):1200–4, April 2011.

[79] Chun Huang, Matthew M. Sartin, Nisan Siegel, Matteo Cozzuol, Yadong Zhang, Joel M. Hales, Stephen Barlow, Joseph W. Perry, and Seth R. Marder. Photo-induced charge transfer and nonlinear absorption in dyads composed of a two-photon-absorbing donor and a perylene diimide acceptor. *Journal of Materials Chemistry*, 21(40):16119, 2011.

[80] Fritjof Helmchen and Winfried Denk. Deep tissue two-photon microscopy. *Nature methods*, 2(12):932–40, December 2005.

[81] Chandan Biswas, Hyun Jeong, Mun Seok Jeong, Woo Jong Yu, Didier Pribat, and Young Hee Lee. Quantum Dot-Carbon Nanotube Hybrid Phototransistor with an Enhanced Optical Stark Effect. *Advanced Functional Materials*, pages n/a–n/a, February 2013.

[82] Hongsik Park, Ali Afzali, Shu-Jen Han, George S Tulevski, Aaron D Franklin, Jerry Tersoff, James B Hannon, and Wilfried Haensch. High-density integration of carbon nanotubes via chemical self-assembly. *Nature nanotechnology*, 7(12):787–91, December 2012.

[83] Lapo Bogani and Wolfgang Wernsdorfer. Molecular spintronics using single-molecule magnets. *Nature materials*, 7(3):179–86, March 2008.

[84] Marc Ganzhorn, Svetlana Klyatskaya, Mario Ruben, and Wolfgang Wernsdorfer. Strong spin-phonon coupling between a single-molecule magnet and a carbon nanotube nanoelectromechanical system. *Nature nanotechnology*, (February):1–5, February 2013.

[85] Pascal Bluemmel. *Solubilization and Individualization of Carbon Nanotubes by Noncovalent Functionalization with Switchable Molecules*. Diplomarbeit, Freie Universität Berlin, 2009.

For copyright reasons, the five publications comprising this cummulative thesis are not included in the online version. The publications are listed below together with their digital object identifiers.

1. Energy Transfer in Nanotube-Perylene Complexes
   F. Ernst, T. Heek, A. Setaro, R. Haag, and S. Reich
   Adv. Funct. Mater. **22**, 3921-3926 (2012).
   http://dx.doi.org/10.1002/adfm.201200784

2. Chirally enhanced solubilization through perylene-based surfactant
   F. Ernst, T. Heek, R. Haag, S. Reich, and A. Setaro
   Phys. Status Solidi (b) **249**, 2465-2468 (2012).
   http://dx.doi.org/10.1002/pssb.201200192

3. Functional Surfactants for Carbon Nanotubes: Effect of Design
   F. Ernst, T. Heek, A. Setaro, R. Haag, and S. Reich
   J. Phys. Chem. C **117**, 1157-1162 (2013).
   http://dx.doi.org/10.1021/jp3098186

4. Excitation characteristics of different energy transfer in nanotube-perylene complexes
   F. Ernst, T. Heek, A. Setaro, R. Haag, and S. Reich
   Appl. Phys. Lett. **102**, 233105 (2013).
   http://dx.doi.org/10.1063/1.4810912

5. Selective interaction between nanotubes and perylene based surfactant
   F. Ernst, S. Heeg, T. Heek, A. Setaro, R. Haag, and S. Reich
   Phys. Status Solidi (RRL) **7**, 546-549 (2013).
   http://dx.doi.org/10.1002/pssr.201307221